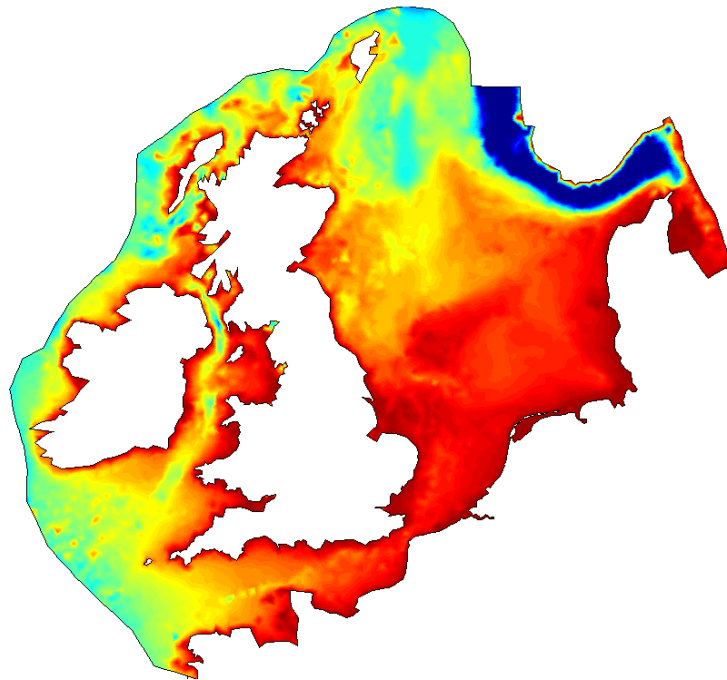# "2D or not 2D?"

Three-dimensional effects in two-dimensional modelling
of oscillatory flow in shelf seas and estuaries

Svašek Hydraulics

Delft University of Technology
Faculty of Civil Egnineering and Geosciences
Section of Environmental Fluid Mechanics

MSc thesis
Delft University of Technology

"2D or not 2D?"

**Three-dimensional effects in
two-dimensional modelling of oscillatory flow
in shelf seas and estuaries**

Frederieke DOORN
March 3, 2014

Graduation Committee:
prof. dr. ir. W.S.J. UIJTTEWAAL (TU Delft)
dr. ir. R.J. LABEUR (TU Delft)
ir. L. DE WIT (TU Delft)
ir. B.A.J. LES (Svašek)

Abstract

The objective of this study is to develop a theoretical framework to judge in which particular instances a two-dimensional depth-averaged model is sufficient to simulate flow processes in continental shelf seas or when a fully three-dimensional model is required for accurate results. A depth-averaged model does not give any vertical information, which is unfortunate when the model user is interested in it. Moreover, the model output, i.e. the surface elevation and the depth-averaged velocity components, may be affected by omitting the vertical dimension. In a frictionless case, two-dimensional and three-dimensional model results would be equal.

First, it is examined whether the reduction from 3D to 2DH has a significant effect on model output by comparing mathematical models with (2DV) and without (1D) vertical information. Localized analytical solutions are derived for the propagation of a single (predominant) tidal constituent in a shallow well-mixed continental shelf sea or estuary. The advective and Coriolis terms are neglected, the eddy viscosity is assumed constant and the bottom friction term is linearised. Special attention is paid to the latter, since both 1D and 2DV responses appear to depend substantially on the way the bottom friction coefficients are defined.

The analytical method developed in this study indicates that certain combinations of the higher flow velocities ($\hat{U} > 1$ m/s) and water depths ($d > 50$ m) may cause extensive differences between the results from a depth-averaged model and from a model that contains vertical information. However, it should be kept in mind that those two parameters interact and hence conclusions in general sense are hard to quantify.

The resulting findings are tested by conceptual numerical simulations of steady and unsteady, periodic flows in a schematized rectangular basin. The results obtained from a three-dimensional simulation are compared to those from a two-dimensional depth-averaged simulation. Both simulations show good correspondence with the analytical solutions.

As the development of the study is motivated by practical problems in the North Sea, its implementation is tested using the European Continental Shelf Model in both two-dimensional and three-dimensional version. A simple iteration procedure is performed to investigate what regions in the flow domain may be important. After an orienting 2D calculation a reasonably simple post-processing step reveals interesting locations where 2D and 3D results are expected to deviate strongly. For these specific locations the performance of the numerical models is analysed and compared.

The case study confirms that the modeller needs to be careful when it comes to two-dimensional depth-averaged hydrodynamic modelling of large-scale domains like the European Continental Shelf Sea. For tidal propagation through large parts of the Central North Sea the flow velocities are rather low ($\hat{U} \approx 0.2$ m/s) and hence two-dimensional (depth-averaged) models are adequate to calculate flow velocities. For several other regions though, being the English Channel, the Irish Sea and around the Orkney Islands, it is shown that it is required to be prudent with interpreting the two-dimensional results.

Acknowledgements

Contents

List of Figures

List of Tables

Nomenclature

Roman Symbols

Symbol	Description	Unit
T	Wave period	[s]
U	Depth-averaged flow velocity in x-direction	[m]
c	Propagation speed	[m/s]
c_{f1}, c_{f2}	Friction coefficients for 1D and 2DV-model respectively	[-]
d	Water depth	[m]
f	Coriolis parameter	[rad/s]
g	Gravitational acceleration	[m/s^2]
p	Pressure	[m^2/s^2]
u, v	Horizontal flow velocities (in x- and y-direction respectively)	[m/s]
$\bar{u}$	Depth-averaged flow velocity in x-direction	[m/s]
$\hat{u}$	Flow velocity amplitude in x-direction	[m/s]
u'	Fluctuating component of flow velocity in x-direction	[m/s]
u_b	Velocity at the bed	[m/s]
w	Vertical flow velocity	[m/s]
x, y	Horizontal spacial coordinates	[m]
z	Vertical spacial coordinate	[m]

Greek Symbols

Symbol	Description	Unit
$\tilde{\gamma}$	Complex parameter	[-]
ϵ	Turbulence dissipation rate	[m^2/s^3]
ζ	Water level elevation	[m]
θ	Time stepping parameter	[-]
κ	Von Karman constant	
κ_1, κ_2	Friction coefficients for linear 1D and 2DV-model respectively	[-]
μ	Dynamic viscosity	[kg/ms]
ν	Kinematic viscosity	[m^2/s]
ν_t	Turbulent eddy viscosity	[m^2/s]
ρ	Density	[kg/m^3]
σ_1, σ_2	Ratio of friction to inertia ratio for 1D and 2DV-model respectively	[-]
τ_b	Bed shear-stress	[N/m^2]
ϕ	Latitude	[°]
ω	Frequency	[rad/s]

Abbreviations

Abbr.	Description
1D, 2D, 3D	One-, Two-, Three-dimensional
2DH	Two-dimensional in horizontal plane (depth-averaged)
2DV	Two-dimensional in vertical plane
ADCP	Accoustic Doppler Current Profiler
CFL	Courant-Friedrichs-Lewy (number)
CG/DG	Continuous/Discontinuous Galerkin (method)
ECSM	European Continental Shelf Model
FEM	Finite Element Method
FINEL	FINite ELements (model)
Fr	Froude number
GIS	Galerkin Interface Stabilization (method)
RANS	Reynolds-Averaged Navier-Stokes (equations)
Re	Reynolds number
SWE	Shallow Water Equations

Chapter 1

Introduction

1.1 Background

The prediction of the behaviour of water masses subjected to winds, waves, currents and tides is essential for many types of hydraulic engineering, ranging from the design of oil platforms to the construction of coastal protection works. Hydrodynamic models are widely used to predict this behaviour, as exact measurement of the hydrodynamics is tedious and costly.

A numerical model is an attempt to represent nature by having a computer solve a set of equations that are thought to describe the natural processes. As Fischer (1979) explains, this attempt cannot be completely successful, because nature itself is marvellously complex and defies exact simulation. The numerical simulation of the real world always means one has to compromise between exact model fit and model simplicity. The main challenge of computational modelling is to describe complex reality by an as simple as possible model. In the case of simulating hydrodynamic processes, first describing the physics with a mathematical model may imply a loss of information because of simplifying assumptions. Subsequently, even more information is lost once the mathematical model is converted into a numerical model. This is shown schematically in the flow chart of figure 1.1, where each of the black arrows imply a loss of information. The modeller must determine which aspects of the real world are important, and must be sure that these aspects are simulated correctly by the model.

Three-dimensional models for the prediction of water-system behaviour exist, but have as a major challenge that they are of such complexity that it brings limitation in both computational capacity as well as human analytical capacity. Consequently, often two-dimensional or even one-dimensional models are used, under the assumption that the variation in the omitted dimension has a limited effect on model output. Whether or not the use of a two-dimensional model is justified in a specific situation depends on various factors, among which certainly is the water depth. The industry wishes an overview of these factors and some guidelines that will indicate until what extent one can comfortably model in two dimensions.
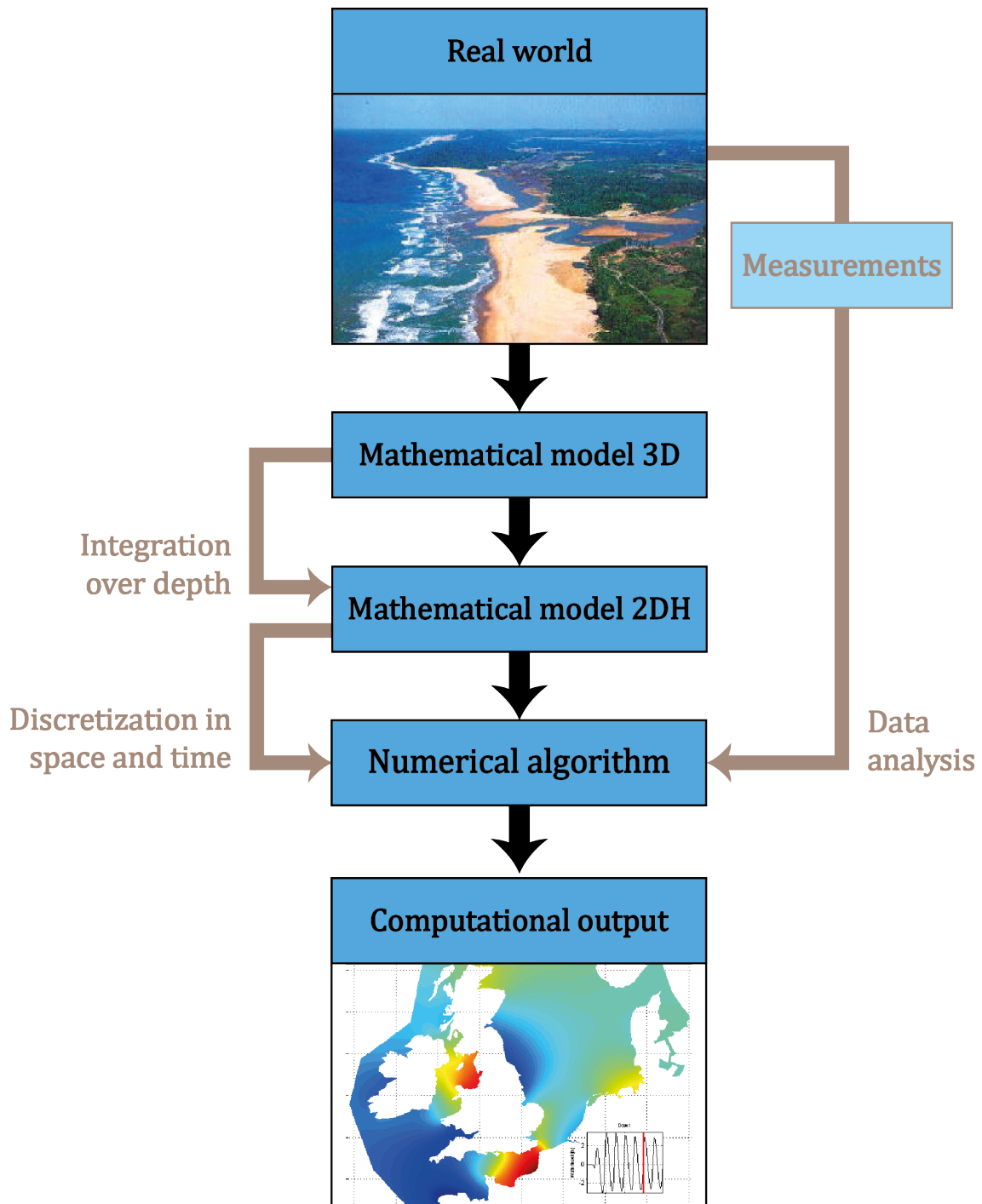
Figure 1.1: *Flow chart of stages in computational hydraulics as used in this study for large-scale domains. The first box contains the real world of which a model is to be set up, i.e. shelf seas or estuaries for this research. The succeeding two boxes contain the mathematical spaces that describe the real world with conservation laws, i.e. continuity and momentum equations for this research. Next is the discrete space where differential equations are replaced by recurrence relations which are solved. The final box contains the computational model output calculated by the computer.*

1.2 Problem statement

The main question that will be addressed in this research is when it becomes essential to take into consideration three-dimensional effects in the hydrodynamics of shelf seas and estuaries. Two-dimensional hydrodynamic models have proven to be capable of simulating flow and transport processes in rivers, lakes, estuaries, deltas and continental shelf seas. Practice shows that even when significant three-dimensional effects are expected, such as in wind-driven flows, the two-dimensional approach may work extremely well. However, there are cases where a two-dimensional model is not sufficiently representing the actual flow structures. For example, in continental shelf seas close to the shelf edge this is expected to be the case, because complex topography and dynamics might cause the velocity profile to be far from uniform. What is lacking presently, is a decision-making framework on whether to use a two- or a three-dimensional model in such a case. The transition between the use of a two-dimensional model and that of a three-dimensional one when shifting further offshore, is still a rather grey area.

Which degree of loss of predictive power is acceptable depends on the flow problem to be studied and on the required model output. Fluid flow problems have all kinds of length, time and velocity scales, while each application has its own accuracy requirement. This results in a different appropriate approach for each problem. Obviously the physics to be described has three spatial dimensions. Depending on the circumstances several simplifications can be opted in order to describe a flow phenomenon with a one-, two- or three-dimensional mathematical model. In many coastal engineering applications it is often sufficient to apply a two-dimensional horizontal model, based on the shallow-water equations. The shallow-water equations describe nearly-horizontal geophysical flows for which the ratio of the vertical to horizontal velocity magnitudes is very small, so that the pressure can be assumed hydrostatic and the Navier-Stokes equations can be integrated over the water depth. If the horizontal velocity is nearly uniform in the vertical direction, which in many cases is a reasonable assumption, the shallow-water equations provide a good approximation of the original flow problem while offering a substantial reduction in terms of complexity and computational effort.
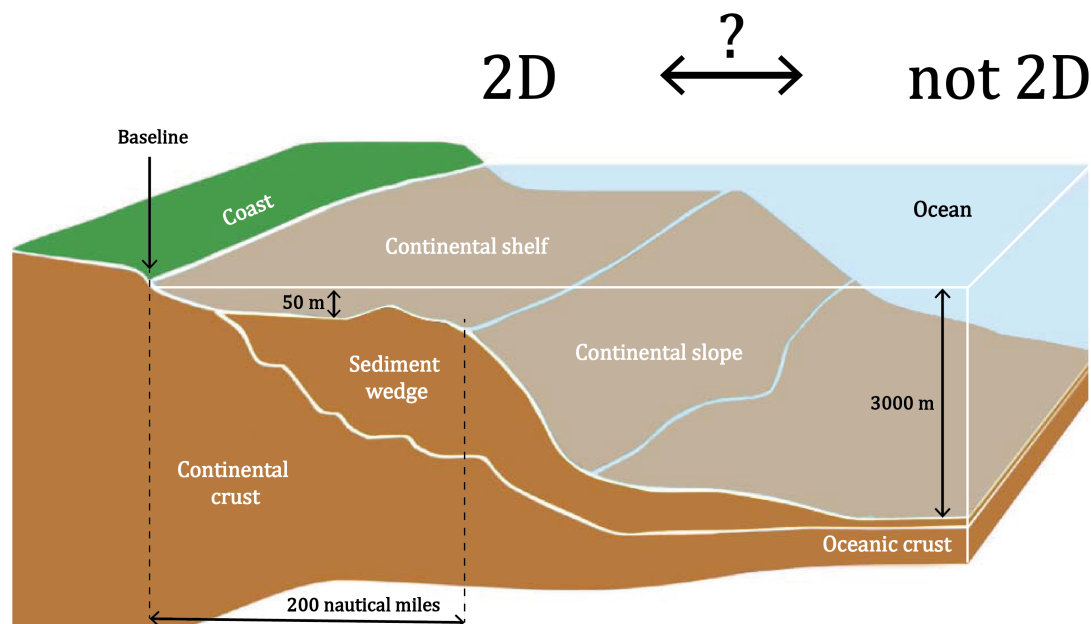
Figure 1.2: *The definition of the continental shelf and criteria for the establishment of its outer limits are set out in article 76 of the UnitedNations (2012) Convention on the Law of the Sea.*

1.3 Objectives

The main objective of this research is:

- "To develop a theoretical framework to judge in which particular instances a two-dimensional model is sufficient to simulate flow processes in continental shelf seas."

To this end, this research will examine whether the reduction from 3D to 2D has a significant effect on flow model output being water levels and depth-averaged flow velocities. The research objective will be achieved by answering the following research questions:

- Which physical processes are relevant in well-mixed continental shelf seas?

- Which simplifications are applied to a flow problem in order to allow the use of two-dimensional depth-averaged rather than three-dimensional shallow-water equations?

- Which parameters are important when a depth-averaged model is compared to a model that contains vertical information.

- In which cases is a depth-averaged two-dimensional model still representative?

1.4 Approach

First, research into the physical processes needs to be carried out. This will be done through a combination of literature study and analytical research. The literature study will enhance the understanding of the three-dimensional flow in shelf seas. The analytical approach has to reveal the effect of averaging over depth through analytical solutions to strongly simplified situations. The function of this mathematical model is tested by different scenarios (1D and 2DV) to establish crude ranges within which the models could be valid.

Next is the numerical modelling of tidal flow in simple geometries to isolate certain processes in line with the preceding analytical approach. The results obtained from a three-dimensional simulation are compared to those from a two-dimensional depth-averaged simulation, and both are compared to the analytical solutions. Merely, the performance of models are discussed for conceptual cases. The analytical background will now be a very useful tool, because it will provide *a priori* knowledge on the importance of parameters.

Subsequently, through a case study in the North Sea the distinctive power of both the two-dimensional model and the three-dimensional model will be tested. For specific locations, where three-dimensional processes might be important, the performance of the numerical models is analysed.

So, this research aims at theory-grounded and evidence-based assessment of the applicability of two- and three-dimensional calculations for both conceptual and real cases and under additional hypothetical simulated circumstances. Ultimately it will result in a better insight into the scope to extend the application of two-dimensional numerical flow models.

1.5 Practical relevance

It could be argued that it is no longer necessary to use two-dimensional models since there is a progression towards increasingly sophisticated three-dimensional models with a higher predictive power. This progression should however be treated with caution for a number of reasons. First, three-dimensional models require a considerable increase in computational resources. Also, it is important to judge the need for improved process representation. As described above, whilst there may be key three-dimensional processes occurring, the two-dimensional depth-averaged shallow-water equations may give the same information. So, the reduction from three dimensions to a two-dimensional model means...

1. ... at least a loss of vertical information (which is unfortunate when the model user is interested in it);

2. ... but perhaps it has an effect on the model output; the water levels and the depth-averaged velocities.

The research is done for the specialist consultant Svašek Hydraulics. Svašek focuses on water dynamics (currents and waves) and sediment transport caused by the water dynamics. Its regions of expertise are coasts and coastal seas, estuaries and rivers. Its clients include government bodies and authorities, contractors, industrial companies and general consultants.

Svašek uses the in-house developed two-dimensional numerical flow model FINEL2D. When calculating the depth-averaged velocity profiles for a client, Svašek wants to be sure that this calculation is fit-for-purpose, to best serve the interest of the client. For many projects this is the case, but especially for cases with water depths larger than ± 50 m it becomes unclear whether the calculated flow represents the real fluid flow. Svašek wants to obtain more knowledge about the limits of applicability of its two-dimensional model in deeper parts of continental shelf seas than they are familiar with so far.

In addition, Svašek has FINEL3D, a fully 3-dimensional numerical model where no assumptions are made with respect to the vertical pressure distribution. Hence, the model is especially suited to compute currents which vary strongly in both horizontal and vertical directions.

1.6 Thesis outline

Chapter 2 describes the physical processes in continental shelf seas and estuaries. This chapter also presents the equations of motion and the relevance of the terms for each of the processes. By assessing the relevance of the terms, the equations of motion are reduced to a workable mathematical model. Chapter 3 contains analytical solutions to this mathematical model. In this chapter, the function of the mathematical model is tested by different scenarios (1D and 2DV) to establish crude ranges within which a depth-averaged model could be valid. Chapter 4 treats conceptual simulations for schematized rectangular basins that are compared to the analytical solutions. Chapter 5 describes a case study containing numerical results from the European Continental Shelf Model.

Chapter 2

Physical processes in shelf seas and estuaries

Continental shelf seas are a natural source of economic activities and other forms of human use, which make hydrodynamic modelling a useful tool for a variety of users. This research focuses on the parts of shelf seas with water depths larger than circa 50 m, such as the northern North Sea. This thesis can function as a tool for the prediction of the conditions for pipeline laying or maintenance of cables or pipelines in such an environment. Further offshore less is known about the behaviour of the characteristic physical phenomena and the suitability of a two-dimensional model in such cases. This chapter describes these phenomena, their characteristic length, time and velocity scales and the governing processes in shelf seas.

Subsequently, the governing equations of motion are discussed and simplified as much as possible based on commonly used assumptions and approximations. Moreover, for each of the relevant phenomena the equations are scaled with characteristic values, which will give insight into which terms of the equations are dominant for which phenomenon. This helps to find out which processes are governing and which of the parameters are responsible for the behaviour. All of this results in a basic three-dimensional mathematical model. Finally, by integration over the water depth the consequences of the reduction from the three-dimensional to the two-dimensional equations are exposed. This results in two sets of basic equations for both 2D and 3D modelling of fluid flow problems under circumstances likely to occur in North Sea like conditions.

2.1 Important phenomena in shelf seas and estuaries

Globally, there are many shelf regions with many different characteristics due to a varying combination of currents, winds and waves. This section treats the most important phenomena for shelf seas and estuaries and aims to define characteristic length, time and velocity scales. Areas of application are tides and wind-driven flows (i.e. storm surges). River flows and stratified or density-driven flows are beyond the scope of this research.

Tides Tidal motion is generated by the gravitational forces of the sun and moon upon the rotating earth. In the ocean, the amplitude of the tide is $\mathcal{O}(0.1m)$ (Holthuijzen, 2007). The propagation speed of the tide is $c = \sqrt{gd}$, where d is the water depth. With $d \approx 3000$ m, the tidal propagation speed in the ocean is 175 m/s (or 600 km/h). The particle velocity, tidal current speed, is much smaller and is related to the water depth and the tidal amplitude via $u = \zeta \sqrt{(g/d)} \approx 0.005$ m/s.

As the tidal wave approaches the relatively shallow continental shelf its amplitude increases to $\mathcal{O}(1m)$ and propagation of the wave is retarded ($\sim$30 m/s). Current speed in these seas may be as high as 0.2 m/s or more. In long, narrow bays or estuaries, resonance may occur and the amplitude may be as high as 15 m with correspondingly high current speeds. In enclosed seas, tides are practically absent (e.g. Mediterranean Sea, Black Sea). All is summarised in table 2.1.

The importance of the earth's rotation in the generation and propagation of tidal waves is illustrated by amphidromic systems like the North Sea. The semi-diurnal tides of the North Sea consist of several amphidromic points where the tidal amplitudes are approximately zero. A good description of many observed tidal characteristics are provided by the so-called Kelvin waves. In the solutions for these waves a factor is found responsible for the decay in wave amplitude away from the boundary.

Storm surges Next to tidal forcing, coastal waters are set in motion by atmospheric forcing. The atmosphere forces shelf seas through winds, and through a modification of the water's buoyancy by evaporation, precipitation and heat fluxes, causing buoyancy-driven flow. Winds, directly driving circulation, are generally making the largest contribution to non-tidal elevations. In the event of water piling up against the coast, this is called a (storm) surge. A typical property of surges is that they behave as a wave, travelling along the coast, of which the amplitude grows with time. The severity of a storm surge depends to a large extent on its timing relative to the tidal cycle. If the peak of the surge coincides with high tide, the effect can be disastrous. A characteristic time scale for storm surges is $1 - 2$ days, so $T \approx 2000$ min would be a reasonable value.

Residual currents In Nihoul and Ronday (1975) the residual current field is defined as the mean velocity field over a time sufficiently long to cover several tidal periods and thus cancel transitory wind currents and tidal oscillations. In deriving appropriate equations for the residual circulation extra non-linear terms appear in the equations of motion due to decomposition of the velocity vector into a time averaged component and a perturbation. In certain regions, as a consequence of intensive tidal oscillations, these non-linear contributions are extremely important and the fluctuating velocity component can be 10 to 100 times larger than the time averaged velocity component. So, a characteristic time scale is several times a tidal period of 745 minutes, resulting in $T \approx 3500$ min.

Seiches Seiches are free oscillations that occur in basins of moderate size (harbours, lakes, bays or even in a sea). They are standing waves with a frequency equal to the resonance frequency of the basin in which they occur. Seiches can have periods ranging from a few minutes up to several hours. As seiches are a resonance phenomenon, it is obvious that the basin size in relation to the wavelength is an important factor.

Density-driven currents Due to variations in temperature or salinity currents may be driven. This is however beyond the scope of this thesis because the focus is on well-mixed shelf seas and estuaries.

2.2   Equations of motion

The three-dimensional Navier-Stokes equations are generally accepted as the mathematical starting point for fluid flow problems. These equations are based on Newton's Second Law and describe the conservation of momentum and mass. Under the assumption of water being an incompressible fluid the latter equation reduces to the continuity equation:

$$\frac{\partial u}{\partial x} + \frac{\partial v}{\partial y} + \frac{\partial w}{\partial z} = 0 \tag{2.1}$$

with velocity components u, v and w in x-, y- and z-direction respectively. The conservation of momentum is expressed as (Pedlosky, 1982):

$$\frac{\partial(\rho u)}{\partial t} + \frac{\partial(\rho u^2)}{\partial x} + \frac{\partial(\rho uv)}{\partial y} + \frac{\partial(\rho uw)}{\partial z} = -\frac{\partial p}{\partial x} + \rho f v + \frac{\partial \tau_{xx}}{\partial x} + \frac{\partial \tau_{xy}}{\partial y} + \frac{\partial \tau_{xz}}{\partial z} \tag{2.2a}$$

$$\frac{\partial(\rho v)}{\partial t} + \frac{\partial(\rho uv)}{\partial x} + \frac{\partial(\rho v^2)}{\partial y} + \frac{\partial(\rho vw)}{\partial z} = -\frac{\partial p}{\partial y} - \rho f u + \frac{\partial \tau_{yx}}{\partial x} + \frac{\partial \tau_{yy}}{\partial y} + \frac{\partial \tau_{yz}}{\partial z} \tag{2.2b}$$

$$\frac{\partial(\rho w)}{\partial t} + \frac{\partial(\rho uw)}{\partial x} + \frac{\partial(\rho vw)}{\partial y} + \frac{\partial(\rho w^2)}{\partial z} = -\frac{\partial p}{\partial z} - \rho g + \frac{\partial \tau_{zx}}{\partial x} + \frac{\partial \tau_{zy}}{\partial y} + \frac{\partial \tau_{zz}}{\partial z} \tag{2.2c}$$

where ρ denotes the density of the water, p the pressure, f the Coriolis parameter and τ_{ij} is the viscous shear stress in i-direction on a j-plane. The stresses are defined as $\tau_{ij} = \rho \nu \left(\frac{\partial u_i}{\partial x_j} + \frac{\partial u_j}{\partial x_i} \right)$, where ν is the kinematic viscosity. A short-hand notation is used where $x_i = (x, y, z)$ and $u_i = (u, v, w)$ for $i = 1, 2, 3$.

The assumption of water being an incompressible fluid does not automatically mean that the fluid density is constant, but rather that it is independent of the pressure. The density may still vary due to other reasons, such as variations in temperature or salinity. Very often though, the variations in density are small with respect to the density itself (usually less than a few percent). Therefore, the density may be taken as a constant ρ_0 in all terms but the buoyancy term, where it is important. The approach of taking density variations into account only in the buoyancy term is called the *Boussinesq approximation*.

In essentially all civil engineering applications the flow is found to be turbulent. Turbulence is a chaotic and fluctuating phenomenon. To account for turbulence in the Navier-Stokes equations the variables are decomposed into a mean and a variation, e.g. $u = \bar{u} + u'$. Substituting the decomposition for all variables into the momentum equations and taking the average results in the Reynolds-averaged equations of motion. These have the same form as the original Navier-Stokes equations, with additional turbulent stresses called *Reynolds stresses*, e.g. $\tau_{ij} = \rho \overline{u_i' u_j'}$ (Uijttewaal, 2011). These turbulent stresses are often found to be many orders of magnitude larger than the viscous stresses, since molecular viscosity is only important within a few millimetres of a boundary.

The Reynolds stresses have to be expressed in terms of the mean motion in order to obtain a closed system of equations. This closure problem is one of the major tasks of turbulence research. A simple turbulence model uses the *Boussinesq hypothesis* to describe the turbulent motions in a similar way to the molecular motions but with eddy viscosity coefficients ν_t^h and ν_t^v for the horizontal and vertical direction respectively. All of the above taken into account results in the following equations:

$$\frac{\partial u}{\partial t} + u\frac{\partial u}{\partial x} + v\frac{\partial u}{\partial y} + w\frac{\partial u}{\partial z} = -\frac{1}{\rho_0}\frac{\partial p}{\partial x} + fv + \frac{\partial}{\partial x}\left(\nu_t^h\frac{\partial u}{\partial x}\right) + \frac{\partial}{\partial y}\left(\nu_t^h\frac{\partial u}{\partial y}\right) + \frac{\partial}{\partial z}\left(\nu_t^v\frac{\partial u}{\partial z}\right) \tag{2.3a}$$

$$\frac{\partial v}{\partial t} + u\frac{\partial v}{\partial x} + v\frac{\partial v}{\partial y} + w\frac{\partial v}{\partial z} = -\frac{1}{\rho_0}\frac{\partial p}{\partial y} - fu + \frac{\partial}{\partial x}\left(\nu_t^h\frac{\partial v}{\partial x}\right) + \frac{\partial}{\partial y}\left(\nu_t^h\frac{\partial v}{\partial y}\right) + \frac{\partial}{\partial z}\left(\nu_t^v\frac{\partial v}{\partial z}\right) \tag{2.3b}$$

$$\frac{\partial w}{\partial t} + u\frac{\partial w}{\partial x} + v\frac{\partial w}{\partial y} + w\frac{\partial w}{\partial z} = -\frac{1}{\rho_0}\frac{\partial p}{\partial z} - \frac{\rho}{\rho_0}g + \frac{\partial}{\partial x}\left(\nu_t^h\frac{\partial w}{\partial x}\right) + \frac{\partial}{\partial y}\left(\nu_t^h\frac{\partial w}{\partial y}\right) + \frac{\partial}{\partial z}\left(\nu_t^v\frac{\partial w}{\partial z}\right) \tag{2.3c}$$

2.3 Boundary conditions

In order to compute changes in the structure of the sea, it is necessary not only to know the governing equations but also the appropriate conditions to apply at the boundaries. Distinction can be made between different types of boundaries: in the horizontal plane and in the vertical plane. In horizontal plane the coastlines are assumed to be a fixed land boundaries, which implies that the velocity normal to the boundary equals zero. Another boundary in the horizontal plane that might have to be imposed because it is not possible to consider the entire sea; the so-called open boundary condition. Typical open boundaries are the edge of the continental shelf, as is treated in chapter 5. In the vertical plane one has to deal with the sea bed and the sea surface. Lastly, there is the boundary condition in time, the initial condition. Important for this research are the vertical boundary conditions.

Depth-averaged flow For depth-averaged flow the shear-stress at the bed induced by a turbulent flow is assumed to be given by a quadratic friction law:

$$\tau_b = \frac{\rho_0 g \, |U| U}{C_1^2} = \rho_0 c_{f1} \, |U| U \tag{2.4}$$

where $|U|$ is the magnitude of the depth-averaged horizontal velocity and C_1 is the Chézy coefficient for a depth-averaged model.

Flow with vertical information For models with vertical information, e.g. 2DV or 3D models, a quadratic bed stress formulation is used that is quite similar to the one for depth-averaged computations. The bed shear stress in 3D may be related to the current just above the bed:

$$\tau_b = \rho_0 c_{f2} |u_b| u_b \tag{2.5}$$

with u_b is the magnitude of the horizontal velocity just above the bed. More on the bottom boundary condition in Chapter 3.

The next section treats a more extensive analysis of the equations of motion, with emphasis on the relative importance of the terms. In chapter 3 the equations are extremely simplified in order to find some analytical solutions.

2.4 Scaling the equations

Within the framework of this research it is inconvenient to work with the full equations, because it makes the succeeding analysis unnecessarily laborious. Implementing characteristic scales for each of the parameters gives insight into which terms in the equations are negligible in which situation. Accordingly, the equations can be simplified to a certain extent.

Firstly, the continuity equation is considered. Suppose U characterises the scales of the horizontal velocities u and v, L characterises the horizontal length scales x and y, and H the vertical scale z. Then, the continuity equation scales leads to an expression for the vertical velocity scale W:

$$\frac{\partial u}{\partial x} + \frac{\partial v}{\partial y} + \frac{\partial w}{\partial z} = 0$$

$$\frac{U}{L} + \frac{U}{L} + \frac{W}{H} = 0 \quad \implies \quad W \sim O\left(\frac{UH}{L}\right)$$
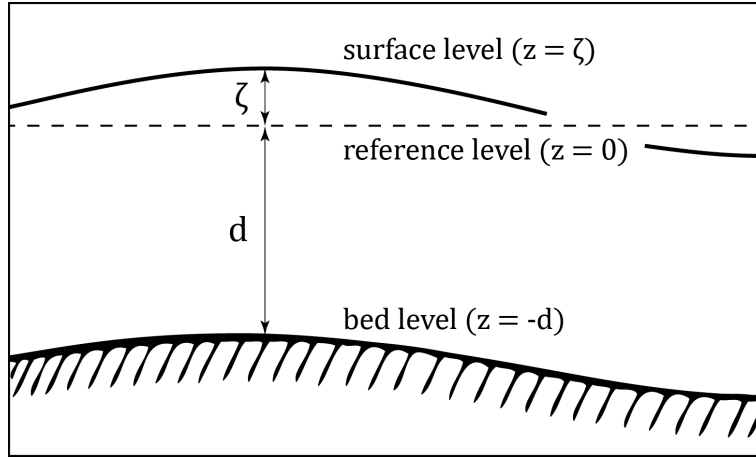
Figure 2.1: *Definition of the surface elevation ζ and the undisturbed water depth d.*

In table 2.1 characteristic time, length and velocity scales are summarised for the physical phenomena discussed in the previous section (partly from Battjes (2002)). It shows that the horizontal velocity component is a few orders of magnitude larger than the vertical velocity component for all relevant phenomena. Therefore, the vertical velocity component can be neglected for the type of applications treated in this research and thus it will not be considered.

Table 2.1: *Characteristic scales for different physical phenomena.*

Type	T [min]	L [m]	H [m]	U [m/s]	W [m/s]
Tide in the ocean	745	10^6	3000	0.3	$9 \cdot 10^{-4}$
Tide in shelf seas	745	10^5	50	0.5	$3 \cdot 10^{-4}$
Tide in estuaries	745	10^3	15	1	$2 \cdot 10^{-2}$
Storm surges	2000	10^5	50	1.5	$8 \cdot 10^{-4}$
Residual currents	3500	10^5	50	2	$1 \cdot 10^{-3}$
Seiches	20	10^3	20	0.5	$1 \cdot 10^{-2}$

Substituting the above scales into the vertical momentum equation 2.3c shows that the only important balance in the vertical is the balance between the pressure gradient and gravity for all of the physical phenomena. The other terms are so small that they can be dropped without changing the dominant characteristics of the solutions. Therefore, the vertical momentum equation reduces to the so-called **hydrostatic balance**:

$$\frac{\partial p}{\partial z} = -\rho g \tag{2.6}$$

Integration of equation 2.6 in vertical direction gives: $p(z) = \rho g(\zeta - z) + p_{atm}$ when $\frac{\partial \rho}{\partial z} = 0$, where ζ is the elevation of the free surface (see figure 2.1) and p_{atm} is the atmospheric pressure at the free surface. Now

$$\begin{aligned} \frac{\partial p}{\partial x} = \rho g \frac{\partial \zeta}{\partial x} \\ \frac{\partial p}{\partial y} = \rho g \frac{\partial \zeta}{\partial y} \end{aligned} \quad \text{if} \quad \frac{\partial \rho}{\partial x}, \frac{\partial \rho}{\partial y} = 0 \tag{2.7a}$$

Substituting this into the horizontal momentum equations 2.3a and 2.3b gives:

$$\frac{\partial u}{\partial t} + u\frac{\partial u}{\partial x} + v\frac{\partial u}{\partial y} - \frac{\partial}{\partial z}\left(\nu_t \frac{\partial u}{\partial z}\right) = -g\frac{\partial \zeta}{\partial x} + fv \tag{2.8a}$$

$$\frac{\partial v}{\partial t} + u\frac{\partial v}{\partial x} + v\frac{\partial v}{\partial y} - \frac{\partial}{\partial z}\left(\nu_t \frac{\partial v}{\partial z}\right) = -g\frac{\partial \zeta}{\partial y} - fu \tag{2.8b}$$

Together with neglecting the vertical velocity component and substituting the water level gradient for the pressure gradient, a few other terms were neglected in order to get from equations 2.3a and 2.3b to the above set of equations. The turbulent stresses are often found to be many orders of magnitude larger than the viscous stresses, since molecular viscosity only is important within a few millimetres of a boundary. Therefore the viscous stresses are not taken into account. Also, the horizontal turbulent stresses are not taken into account.

Equations 2.8 are taken as the starting point. The succeeding analysis aims to examine the relative orders of magnitude rather than the exact magnitude of the terms. The essence is to gain insight into the parameters that decide which contributions are the most important in a certain situation and also, which are negligible, and why.

Looking at the terms separately and scaling them with the above discussed length, time and velocity scales:

Inertia: $\quad\quad\quad\quad\quad\quad\quad\quad\quad\quad\quad\quad \frac{\partial u}{\partial t} \sim \frac{U}{T}$

Advection: $\quad\quad\quad\quad\quad\quad\quad\quad\quad\quad u\frac{\partial u}{\partial x} \sim \frac{U^2}{L}$

Vertical diffusion of momentum: $\quad \frac{\partial}{\partial z}\left(\nu_t \frac{\partial u}{\partial z}\right) \sim \nu\frac{U}{H^2}$

Pressure gradient: $\quad\quad\quad\quad\quad\quad\quad -g\frac{\partial \zeta}{\partial x} \sim g\frac{\Delta H}{L}$

Coriolis: $\quad\quad\quad\quad\quad\quad\quad\quad\quad\quad\quad fv \sim fU$

An extremely important term in this research is the friction term, because this term is defined differently in a two-dimensional model. A comparison will be made in the next section. For a three-dimensional model the ratio between the *friction term* and the *inertia term* can be expressed as:

$$\frac{friction}{inertia} \sim \frac{\nu U/H^2}{U/T} \sim \frac{\nu}{\omega H^2}, \quad\quad \text{where} \quad \omega \sim \frac{1}{T} \tag{2.9}$$

This shows that important parameters are the viscosity ν, the wave frequency ω and a vertical length scale (e.g. the water depth d). Vreugdenhil, C.B. (1994) already discussed a dimensionless combination of these parameters: $\omega d^2/\nu$. This dimensionless parameter is used extensively in the analytical approach in the next chapter. Vreugdenhil compares a dynamic expression for the bed shear stress with an expression where the bottom stress is proportional to the depth-averaged velocity as in a steady state. The result is a ratio, shown in figure 2.2, as a function of this parameter $\omega d^2/\nu$ only.

When $\omega d^2/\nu$ is very small, the ratio approaches unity, which means that the bed shear stress responds to the periodic flow as if it were steady at each moment. For approximately $\omega d^2/\nu < 0.5$ this is the case. This can also be written as $d^2/\nu < 0.5\cdot T/2\pi \approx 0.08\cdot T$, where T is the period of the oscillating flow. The quantity d^2/ν can be interpreted as the time needed for a viscous flow to adjust its velocity profile over a depth d. So, a quasi-steady bed shear stress is expected when the adjustment time is less than 8% of the period.

In the case of homogeneous tidal flow vertical mixing is predominantly caused by turbulence generated by bed shear stress. For turbulent flow in shallow water an estimate for the eddy viscosity is $\nu = \frac{1}{6}\kappa d u_\star = 0.067 d u_\star$ (Fischer, 1979). Here, $u_\star \approx \sqrt{c_f}\cdot\bar{u}$, and with 0.0015 as an
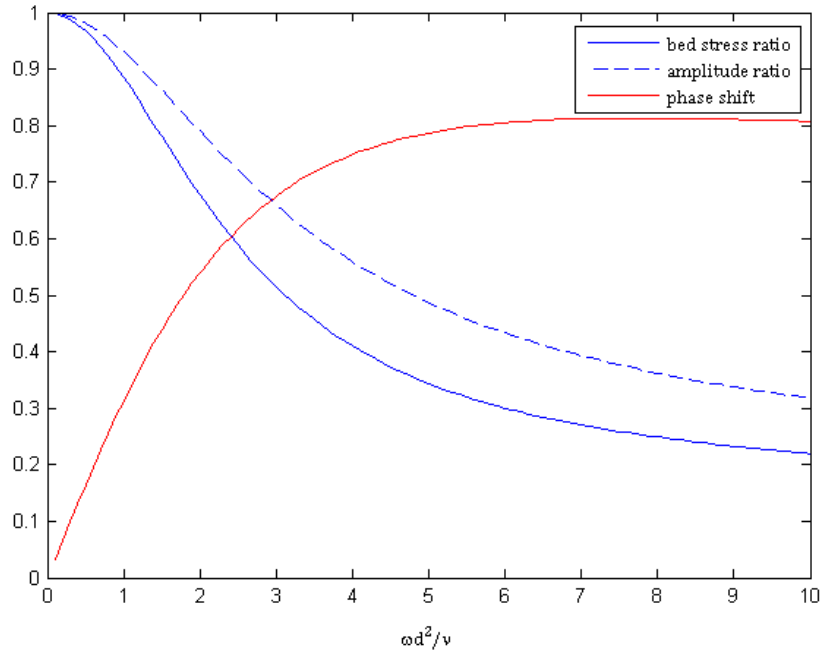
Figure 2.2: *Bed shear stress ratio in dynamic and steady flow.*

estimate for c_f it becomes $\nu = 0.0025d\bar{u}$. Now, for a homogeneous shelf sea such as the North Sea, with an average water depth $d \approx 50$ m and a depth mean amplitude of the current $\bar{u} \approx 0.5$ m/s, an estimate for the eddy viscosity $\nu \approx 0.063$ m^2/s. Then, the adjustment time becomes 89% of the tidal period, so the quasi-steady assumption breaks down ($\omega d^2/\nu = 5.6$).

2.5 Concluding remarks

Shallow well-mixed continental shelf seas like the North Sea are dominated by strong currents produced by tides and storm surges ($\mathcal{O}(1m/s)$), combined with slowly varying residual currents. These long waves have a characteristic horizontal length scale much greater than the depth, which reduces the vertical momentum equation to the hydrostatic balance. Further analysis of the horizontal momentum equations reveal important parameters for this research: the viscosity ν, the wave frequency ω and the water depth d. The next chapter will confirm this importance by presenting analytical solutions to a depth-averaged (1D) model and a model that does contain information in the vertical (2DV).

Chapter 3

Analytical study

This chapter studies the basic equations obtained in the previous chapter in more detail, by focusing on the difference between the depth-averaged velocities as computed by a 1D and a 2DV model respectively. This analytical approach determines the applicability of 1D and 2DV mathematical models by analysing solutions to the basic equations of motion. As described in the introductory chapter there are two main consequences of using a depth-averaged model instead of a model that does contain information in the vertical direction:

1. A depth-averaged model does not give any vertical information (which is unfortunate when the model user is interested in it);

2. The model output (i.e. the surface elevation and the depth-averaged velocity components) may be affected by omitting the vertical dimension.

This chapter essentially deals with the second issue: it examines whether the reduction from 2DV to 1D (or from 3D to 2DH) has a significant effect on the model output in terms of the surface elevation and depth-averaged current velocities. In order to do so, mathematical models with (2DV) and without (1D) vertical information are compared. Section 3.1 further simplifies the equations of motion that were introduced in the previous chapter. Sections 3.2 and 3.3 study the dynamic response of the vertical velocity profiles to pressure gradient with a 1D and a 2DV mathematical model respectively. A comparison between the two requires more understanding on the bottom shear stress, which is discussed in section 3.4. In section 3.5 the surface elevation is discussed and in section 3.6 two examples are treated.

3.1 Governing equations

Analytical solutions may only be obtained for much simplified forms of the equations of motion. Since the advection terms are non-linear, it is necessary to eliminate them from the momentum equation for this chapter's analytical approach. When the wave propagation speed is defined as the wave length over the wave period ($c = L/T$) the ratio between the *advection term* and the *inertia term* leads to the Froude number, defined as $Fr = u/c$. When $Fr \ll 1$, this means that the inertia term is much more important than the advection term and therefore the advection term may be neglected. This is the case for long waves with small amplitudes with respect to the water depth. The set of equations without advection terms reduces to:

$$\frac{\partial u}{\partial t} - \nu_t \frac{\partial^2 u}{\partial z^2} = -g\frac{\partial \zeta}{\partial x} + fv \tag{3.1a}$$

$$\frac{\partial v}{\partial t} - \nu_t \frac{\partial^2 v}{\partial z^2} = -g\frac{\partial \zeta}{\partial y} - fu \tag{3.1b}$$

$$\frac{\partial p}{\partial z} = -\rho g \tag{3.1c}$$

These are the basic three-dimensional equations for this chapter. From here on periodic flow confined to one horizontal dimension will be considered, given by equation 3.1a; the focus will be on the influence of the variations in the (x,z)-plane. Although tidal vectors generally describe a elliptical path due to the rotation of the earth, Coriolis is neglected in this analytical approach. With these assumptions taken into account the basic 2DV equation for this chapter becomes:

$$\boxed{\frac{\partial u}{\partial t} - \nu_t \frac{\partial^2 u}{\partial z^2} = F} \tag{3.2}$$

where F is just a shorthand notation for the forcing pressure term:

$$F = -g\frac{\partial \zeta}{\partial x} \tag{3.3}$$

In x-direction this term is a scalar, but it may vary in time. With equation 3.2 and the boundary conditions discussed in Chapter 2 analytical solutions are found for the current velocity u. First, the one-dimensional case is considered, where there is no information in the vertical direction.

3.2   1D analytical solution

Equation 3.2 can be integrated over the water depth d in order to get to the one-dimensional momentum equation in x-direction:

$$d\frac{\partial U}{\partial t} - \nu_t \left(\frac{\partial \tilde{u}}{\partial z}\bigg|_{(z=0)} - \frac{\partial \tilde{u}}{\partial z}\bigg|_{(z=-d)} \right) = Fd \tag{3.4}$$

where U is the depth-averaged velocity. At the sea surface ($z = 0$) the shear stress is zero, as the free surface does not produce any friction (in absence of wind). At the bed ($z = -d$) it is common to relate the shear stress term to the depth-averaged velocity with a friction coefficient c_{f1} for the depth-averaged model. So, $\nu_t \frac{\partial u}{\partial z} = \tau_b \approx c_{f1} |U|U$ and the basic one-dimensional **depth-averaged equation** becomes:

$$\boxed{\frac{\partial U}{\partial t} + \frac{c_{f1} |U|U}{d} = F} \tag{3.5}$$

Here, the friction term is proportional to $|U|U$ and therefore non-linear. Since linear equations are much easier to solve analytically, it is convenient to apply a linearisation technique in this matter. Lorentz (1926) proposed this linearisation of the bed shear stress which has been the basis for simple solutions for many decades. Suppose that the flow velocity is varying sinusoidally in time:

$$U(t) = \hat{U} \cos(\omega t) \tag{3.6}$$

where only the real part is considered here from the expression for U that is used further on. Figure 3.1 shows the corresponding $|U|U/\hat{U}^2 = |\cos(\omega t)|\cos(\omega t)$, which is the friction as a function of time that is showing deviations from the pure cosine function.
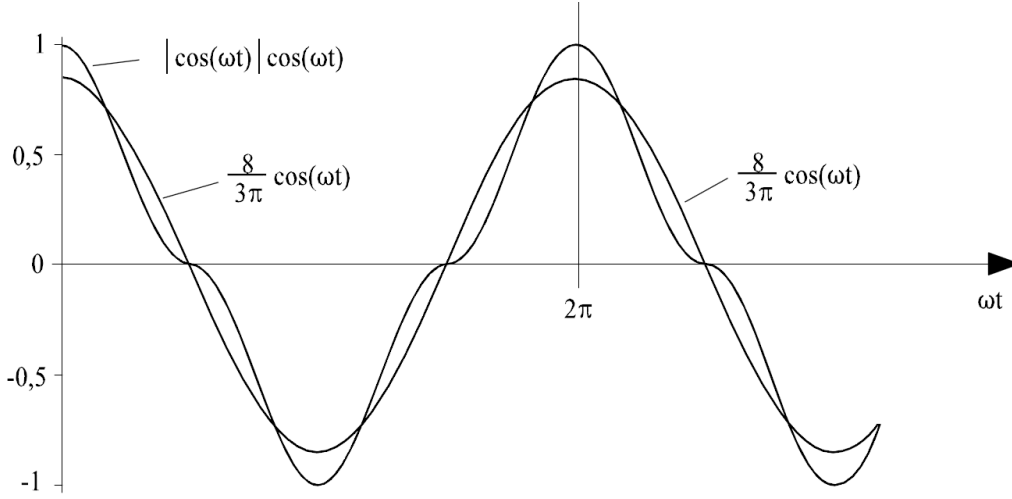
Figure 3.1: *Linearisation of the quadratic friction term (Battjes, 2002).*

The reasoning behind the linearisation lies in the fact that it is accepted that it does not reproduce the exact cosine function, as long as the damping effect of the friction stays conserved. To this end, the energy that is lost per cycle by friction is set to be equal for both cases. This approach works out to a suitable estimate of the linearisation constant κ:

$$\kappa_1 = \frac{8}{3\pi}c_{f1}\frac{\hat{U}}{d} \approx c_{f1}\frac{|U|}{d} \tag{3.7}$$

where the subscript "1" indicates the one-dimensional case. This expression contains a reference velocity $\hat{U}$, which is unknown. Although iterative approaches for its determination have been proposed, this linearisation constant is often assumed as a calibration parameter. With the numerical modelling of schematized rectangular basins of chapter 4 it is done iteratively.

The linearised bed shear stress becomes:

$$\tau_b = c_{f1}|U|U \approx \kappa_1 dU \tag{3.8}$$

Substituting this into equation 3.5 gives:

$$\boxed{\frac{\partial U}{\partial t} + \kappa_1 U = F} \tag{3.9}$$

For dynamic flow in the one-dimensional situation this linearised equation is used, while substituting a complex representation of the flow velocity:

$$U(t) = \tilde{U}e^{i\omega t} \tag{3.10}$$

where $\tilde{U}$ is the complex amplitude and $e^{i\omega t} = \cos(\omega t) + i\sin(\omega t)$ with i is the imaginary unit that satisfies the equation $i = \sqrt{-1}$. This factor $e^{i\omega t}$ actually causes a rotation in time with ω as the angular frequency which equals $2\pi/T$. Observe that the velocity defined in 3.6 equals the real part of this expression: $U(t) = \text{Re}\left[\tilde{U}e^{i\omega t}\right] = \hat{U}\cos(\omega t)$. Substituting the complex periodic

solution 3.10 into equation 3.9 and eliminating the time variation $e^{i\omega t}$ in every term gives:

$$i\omega\tilde{U} + \kappa_1\tilde{U} = \tilde{F} \tag{3.11a}$$

$$(i\omega + \kappa_1)\tilde{U} = \tilde{F} \tag{3.11b}$$

$$\implies \tilde{U} = \frac{\tilde{F}}{(i\omega + \kappa_1)} \tag{3.11c}$$

$$= \frac{\tilde{F}}{i\omega} \cdot \frac{1}{1 + \kappa_1/i\omega} = \tilde{A} \cdot \frac{1}{1 - i\sigma_1} \tag{3.11d}$$

where

$$\tilde{A} = \frac{\tilde{F}}{i\omega} = -\frac{g}{i\omega}\frac{\partial\tilde{\zeta}}{\partial x} \tag{3.12a}$$

$$\sigma_1 = \frac{\kappa_1}{\omega} = \frac{8}{3\pi}c_{f1}\frac{\hat{U}}{\omega d} \tag{3.12b}$$

So, the expression for the depth-averaged velocity in x-direction is:

$$\boxed{U = \tilde{A} \cdot \left(\frac{1}{1 - i\sigma_1}\right) e^{i\omega t}} \tag{3.13}$$

Now, an expression is found for the depth-averaged velocity U through solving a depth-averaged momentum equation. For this research it is interesting to compare this expression with a similar solution for the depth-averaged velocity computed by a model **with** vertical information (2DV).

3.3   2DV analytical solution

Recalling the momentum equation with vertical information (equation 3.2):

$$\frac{\partial u}{\partial t} - \nu_t\frac{\partial^2 u}{\partial z^2} = F \tag{3.14}$$

with a periodic solution $u(z,t) = \tilde{u}(z)e^{i\omega t}$ (now $\tilde{u}$ is the complex amplitude as function of the vertical coordinate), and eliminating $e^{i\omega t}$ this becomes:

$$i\omega\,\tilde{u}(z) - \nu_t\frac{\partial^2}{\partial z^2}\tilde{u}(z) = \tilde{F} \tag{3.15}$$

which is a differential equation with a homogeneous and a particular solution:

$$\tilde{u}(z) = C_1 e^{bz} + C_2 e^{-bz} + \tilde{A} \tag{3.16}$$

where $b = \sqrt{\frac{i\omega}{\nu_t}}$ and $\tilde{A} = \frac{\tilde{F}}{i\omega}$.

At the sea surface ($z = 0$), the shear stress $\tau = 0$, as the free surface does not produce any friction (in absence of wind). So

$$\frac{\partial\tilde{u}}{\partial z}_{(z=0)} = 0 \quad\implies\quad C_1 = C_2 \tag{3.17a}$$

$$\implies \tilde{u}(z) = C\cosh(bz) + \tilde{A} \tag{3.17b}$$

There are several options for the boundary condition at the bed in order to find an expression for the integration constant C. The one discussed in this research is the partial-slip condition,

which means that the velocity at the bed $u_b \neq 0$. At the bed $(z = -d)$, the shear stress is assumed to be described by the linearised quadratic friction law:

$$\nu_t \frac{\partial \tilde{u}}{\partial z}_{(z=-d)} = \tau_b \approx \kappa_2 \, d\tilde{u}, \tag{3.18}$$

where

$$\kappa_2 = \frac{8}{3\pi} c_{f2} \frac{\hat{u}_b}{d} \tag{3.19}$$

The subscript "2" indicates the two-dimensional case. Substituting the expression for the flow velocity (3.17b) in equation 3.18 gives:

$$\nu_t \cdot (C \, b \sinh(-bd)) = \kappa_2 \, d \cdot \left(C \cosh(-bd) + \tilde{A} \right) \tag{3.20a}$$

$$C \cdot (-\nu_t b \sinh(bd) - \kappa_2 \, d \cosh(bd)) = \kappa_2 \, d\tilde{A} \tag{3.20b}$$

$$\implies C = -\tilde{A} \cdot \left(\frac{\nu_t b}{\kappa_2 d} \sinh(bd) + \cosh(bd) \right)^{-1} \tag{3.20c}$$

The solution for the velocity profile in the vertical now becomes:

$$\tilde{u}(z) = \tilde{A} \left(1 - \frac{\cosh(bz)}{\frac{\nu_t b}{\kappa_2 d} \sinh(bd) + \cosh(bd)} \right) \tag{3.21a}$$

$$= \tilde{A} \left(1 - \tilde{\gamma} \frac{\cosh(bz)}{\cosh(bd)} \right) \tag{3.21b}$$

where

$$\tilde{\gamma} = \left(1 + \frac{\nu_t b}{\kappa_2 d} \tanh(bd) \right)^{-1} = \left(1 + \frac{i}{\sigma_2 \, bd} \tanh(bd) \right)^{-1} \tag{3.22}$$

So, the velocity profile described by equation 3.21b is a function of the dimensionless parameter bd:

$$bd = \sqrt{\frac{i\omega d^2}{\nu_t}} \tag{3.23}$$

and the dimensionless σ_2 parameter defined as:

$$\sigma_2 = \frac{\kappa_2}{\omega} = \frac{8}{3\pi} c_{f2} \frac{\hat{u}_b}{\omega d} \tag{3.24}$$

In chapter 2 a similar parameter as the one in equation 3.23 was already discussed in the context of the bed shear stress, indicated as $\omega d^2/\nu_t$ by Vreugdenhil (1994). Figure 3.2 shows the behaviour of the velocity profiles for an increase of this $\omega d^2/\nu_t$-parameter by increasing the water depth. The figures show screen shots of one tidal cycle for water depths of $d = 30, 60, 85$ and 110 m, which corresponds to a $\omega d^2/\nu_t = 1.26, 5.06, 10.16$ and 17.10 respectively, where the eddy viscosity $\nu_t = 0.1$ m^2/s and the tidal frequency $\omega = 1.4 \cdot 10^{-4}$ rad/s are taken constant. Concentrating on the propagation of one single predominant tidal constituent (M$_2$), it is illustrated that an increase in water depth leads to an increase in vertical structure if the viscosity remains constant.

For the depth-averaged velocity the following is derived:

$$\bar{u} = \frac{1}{d} \int\limits_{-d}^{0} \tilde{u}(z) \, dz = \frac{1}{d} \int\limits_{-d}^{0} \left(\tilde{A} \left(1 - \tilde{\gamma} \frac{\cosh(bz)}{\cosh(bd)} \right) \right) \, dz = \frac{\tilde{A}}{d} \left[z - \frac{\tilde{\gamma}}{b} \frac{\sinh(bz)}{\cosh(bd)} \right]_{-d}^{0} \tag{3.25a}$$

$$\boxed{\bar{u} = \tilde{A} \cdot \left(1 - \frac{\tilde{\gamma}}{bd} \tanh(bd) \right) e^{i\omega t}} \tag{3.25b}$$
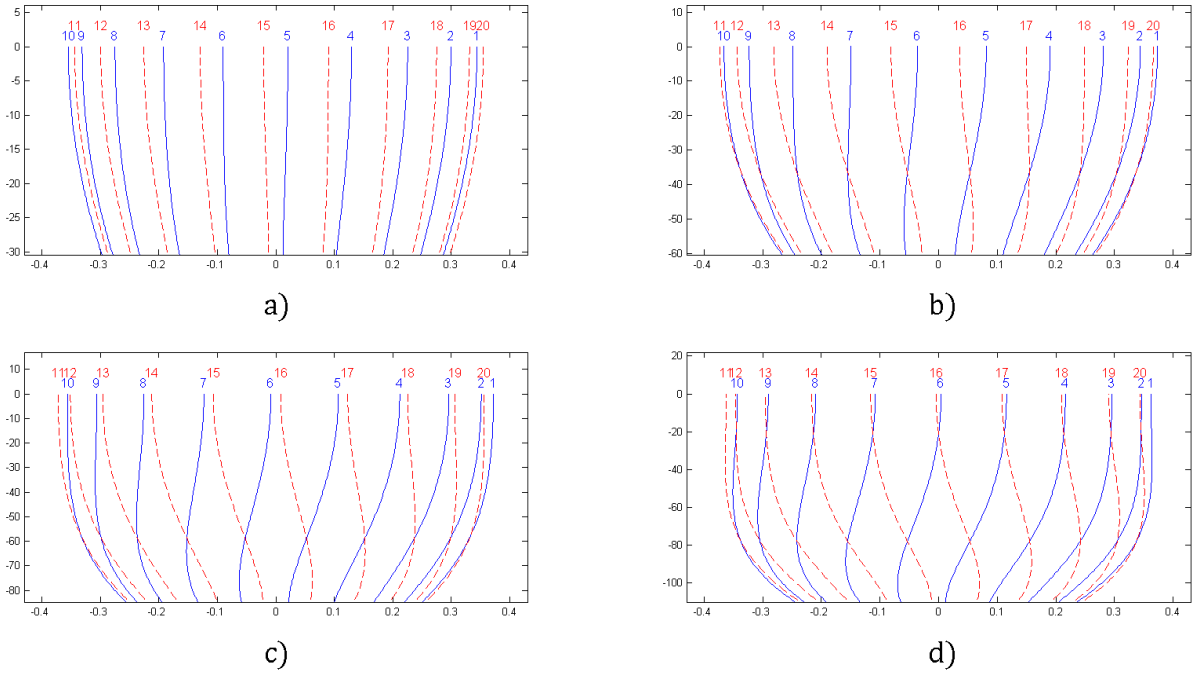
Figure 3.2: *Screen shots of the velocity profiles $u(z)$ over water depths of a) $d = 30$ m, b) $d = 60$ m, c) $d = 85$ m and d) $d = 110$ m for the propagation of one semi-diurnal tidal constituent (M_2, $\omega = 1.4 \cdot 10^{-4}$ rad/s) with a constant vertical eddy viscosity $\nu_t = 0.1$ m^2/s. The figures illustrate one tidal cycle; in solid blue lines the profiles propagating to the left and in dashed red lines to the right.*

3.4 Bottom friction

The preceding sections presented analytical solutions for the depth-averaged flow velocities, as computed by a 1D- and a 2DV-model, both with linearised bottom friction. The expressions for the flow velocities contain two different bottom friction coefficients where $\kappa_1 \neq \kappa_2$ since the bed shear stress is defined differently in both cases. To enable the comparison between these solutions 3.13 and 3.25b, an extra relation between the friction coefficients κ_1 and κ_2 is needed. This relation is found in section 3.4.1 by assuming that for steady flow, which means $\partial u/\partial t = 0$ the depth-averaged velocities computed by both models are equal: $\bar{u} = U$, which is just a matter of choice. The same is done in section 3.4.2, but then for quadratic bottom friction.

3.4.1 Linearised bottom friction

One-dimensional model For steady flow with linearised bottom friction the equation for the 1D-model (3.9) reduces to:

$$\kappa_1 U = F \tag{3.26}$$

where $\kappa_1 \approx c_{f1}|U|/d$ is the linearised friction coefficient for depth-averaged flow (for steady flow the factor $8/3\pi$ is left out), U is the depth-averaged horizontal velocity and $F = -g\partial\zeta/\partial x$, a shorthand notation for the water level gradient. The expression for the depth averaged velocity U follows directly from equation 3.26:

$$\boxed{U = \frac{F}{\kappa_1}} \tag{3.27}$$

Two-dimensional model For steady flow with linearised bottom friction the 2DV-equation (3.2) reduces to:

$$-\nu_t \frac{\partial^2 u}{\partial z^2} = F \tag{3.28}$$

Since F is assumed to be independent of z, integration gives:

$$\nu_t \frac{\partial u}{\partial z} = -Fz + C_1 \tag{3.29}$$

At the sea surface ($z = 0$) the shear stress $\tau_0 = \nu_t \, \partial u / \partial z = 0$, which means that the integration constant $C_1 = 0$ and therefore:

$$\nu_t \frac{\partial u}{\partial z} = -Fz \tag{3.30}$$

So, the shear stress is linearly distributed over the vertical with the maximum shear stress τ_b at the bed ($z = -d$):

$$\tau_b = Fd \tag{3.31}$$

When assuming a constant vertical eddy viscosity the velocity profile is found by integrating equation 3.30:

$$u(z) = C_2 - \frac{Fz^2}{2\nu_t} \tag{3.32}$$

This is a parabolic velocity profile where the integration constant C_2 is equal to the maximum velocity at the sea surface ($z = 0$). To find this constant C_2 a boundary condition needs to be imposed at the bed. Different approaches are possible for the implementation of the bottom boundary condition. This chapter implements the linearised definition for the bottom friction and the numerical modelling chapters 4 and 5 use also a quadratic bottom friction.

The combination of the linearised boundary condition ($\tau_b = \kappa_2 d \, u_b$, where $\kappa_2 \approx c_{f2}|u_b|/d$) and equation 3.31 will result in an expression for the velocity at the bed. Substituting this into equation 3.32 gives an expression for C_2 and so the velocity profile becomes:

$$u(z) = \frac{F}{2\nu_t}\left(d^2 - z^2\right) + \frac{F}{\kappa_2} \tag{3.33}$$

Integrating over depth gives:

$$\bar{u} = \frac{1}{d}\int\limits_{-d}^{0} u(z)\,\mathrm{d}z = \frac{1}{d}\int\limits_{-d}^{0} \frac{F}{2\nu_t}\left(d^2 - z^2\right) + \frac{F}{\kappa_2}\,\mathrm{d}z = \boxed{\frac{Fd^2}{3\nu_t} + \frac{F}{\kappa_2}} \tag{3.34}$$

So, also in the steady case there are two solutions, 3.27 (1D) and 3.34 (2DV), with two different bottom friction coefficients where $\kappa_1 \neq \kappa_2$ since the bed shear stress is defined differently in both cases. Suppose the depth-averaged velocities from both models are equal: $\bar{u} = U$ (which is the method chosen in this study). This results in the following relation between κ_1 and κ_2:

$$\frac{1}{\kappa_1} = \frac{1}{\kappa_2} + \frac{d^2}{3\nu_t} \tag{3.35}$$

Writing this in terms of $\sigma \, (= \kappa/\omega)$:

$$\boxed{\frac{1}{\sigma_1} = \frac{1}{\sigma_2} + \frac{\omega d^2}{3\nu_t}} \tag{3.36}$$

Apparently, in the relation between σ_1 and σ_2 the dimensionless parameter $\omega d^2/\nu_t$ appears. Now, choosing a certain range for σ_1 will result in σ_2 as a function of the dimensionless parameter for every σ_1 value. Typical estimates for $\omega d^2/\nu_t$, σ_1 and σ_2 are given in table 3.1 for the physical phenomena that are relevant for this study.

This σ-relation 3.36 enables a comparison between the amplitudes and phases of the depth-averaged velocities, as computed by a one-dimensional and a two-dimensional model respectively. In figures 3.3 and 3.4 this is done by means of the velocity amplitude and phase ratio for several values for σ_1 indicated in the legend. In these figures the amplitude and phase ratios for the relevant physical phenomena are indicated by dots. Interestingly, in case of tidal motion in the ocean the value of σ_2 becomes negative because of the very large water depth and hence there is no dot in the figure indicating the phenomenon. Since σ is the ratio of the friction to the inertia term, a negative value is physically incorrect. Application of this σ-relation is therefore limited to situations with $\omega d^2/\nu_t > 3/\sigma_1$, which is the case for tidal motion in shelf seas and estuaries.

Concentrating on tides in shelf seas the velocity amplitude ratio is larger than 1 under the condition that $\omega d^2/\nu_t < 65$. This means that the velocity as computed by the depth-averaged model is in much likely to be larger than the velocity amplitude that contains vertical information than vice versa. Furthermore, it is noticed that for shelf seas (the green dot on the line $\sigma_1 = 0.25$) the figures show a velocity amplitude ratio of 1.06 and a phase ratio of 1.01. Apparently, already 6% deviation in amplitudes is expected for parameter values that are very likely to occur in practice. For the same value of $\omega d^2/\nu_t$ but a higher value for σ_1, the differences increase (the red dot on the line $\sigma_1 = 0.50$). The only cause for σ_1 to increase when ω, d and ν_t remain constant would be an increase of the reference velocity $\hat{U}$. So, the initial reference velocity was estimated to be $\hat{U} = 0.5$ m/s for tides in shelf seas, but for $\hat{U} = 1$ m/s the red dot indicates a velocity amplitude ratio of 1.23 and a phase ratio of 0.94.

For smaller values of σ_1 the velocity amplitude ratio is practically always larger than 1 regardless of the value of $\omega d^2/\nu_t$. In case of inertia dominating ($\sigma_1 \ll 1$, i.e. for a seiche for instance), there is hardly any difference to be expected between calculations with and without vertical information. This is indicated by the green dot on the line $\sigma_1 = 0.02$.

The outcome of the amplitude and phase ratios appear to be considerably sensitive to the estimates of the velocity amplitudes $\hat{U}$ presented in table 3.1 as well as to the bottom friction coefficient c_f. Appendix 6 elaborates further on this. Based on the figures above and on the Appendix it can be concluded that the regions where extensive differences are to be expected, e.g. at least 20% for instance, are hard to quantify in general sense. Concentrating on the propagation of the M_2-constituent with a constant vertical eddy viscosity and a certain bottom friction coefficient, much rather it can be stated that there are certain combinations of flow velocity and water depth that may cause the results to differ extremely. This will be tested in the next chapters.

Table 3.1: *Characteristic scales for the dimensionless parameters $\omega d^2/\nu_t$, σ_1 and σ_2 for a constant vertical eddy viscosity $\nu_t = 0.05$ m^2/s.*

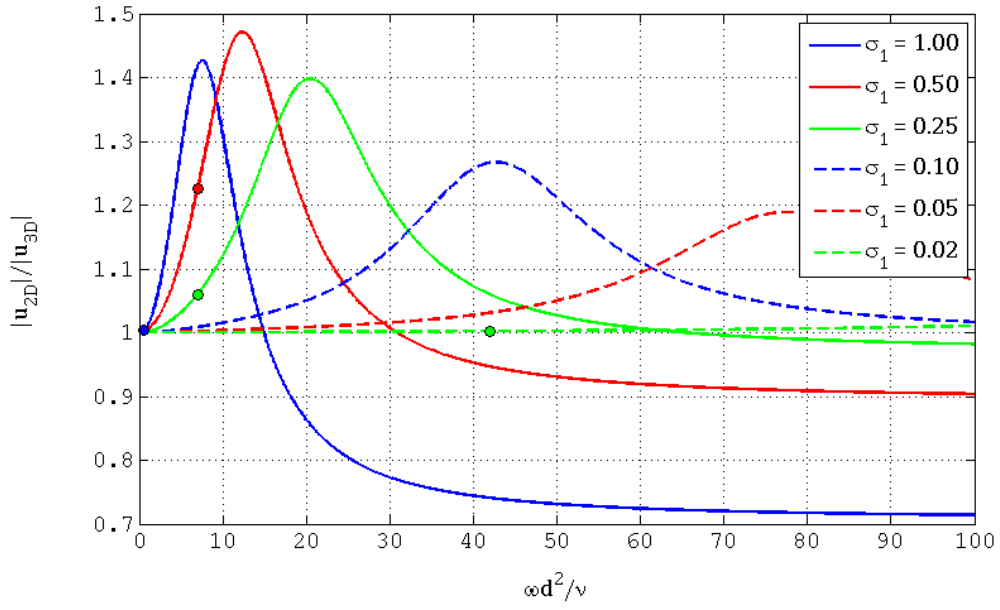| Type	T [min]	ω [rad/s]	d [m]	$\hat{U}$ [m/s]	$\omega d^2/\nu_t$ [$-$]	σ_1 [$-$]	σ_2 [$-$]
Tide in the ocean	745	$1.4 \cdot 10^{-4}$	$4 \cdot 10^3$	0.3	$4 \cdot 10^4$	$2 \cdot 10^{-3}$	$-$
Tide in shelf seas	745	$1.4 \cdot 10^{-4}$	50	0.5	7.0	0.25	0.34
Tide in estuaries	745	$1.4 \cdot 10^{-4}$	15	1.0	0.63	1.00	1.12
Seiches	20	$5.2 \cdot 10^{-3}$	20	0.5	42	0.02	0.02

Figure 3.3: *Amplitude ratio between U and $\bar{u}$ as a function of $\omega d^2/\nu_t$ and σ_1.*
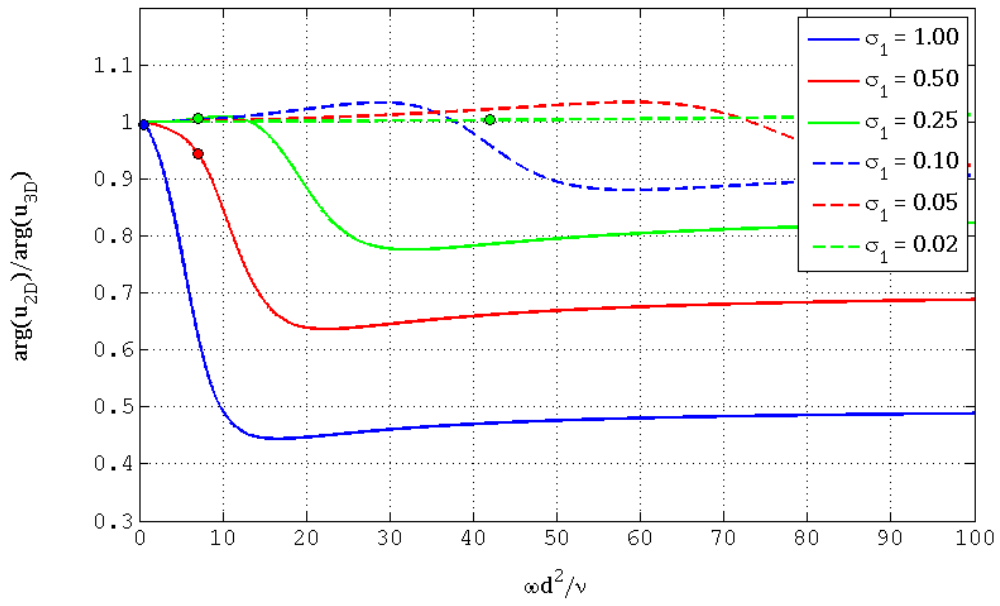
Figure 3.4: *Phase ratio between U and $\bar{u}$ as a function of $\omega d^2/\nu_t$ and σ_1.*

3.4.2 Quadratic bottom friction

Analogous to the preceding section where the relation between κ_1 and κ_2 was derived for the linearised 1D and 2DV-models, this section derives the relation between c_{f1} and c_{f2}. These expressions will be used in the numerical modelling chapter 4 and 5.

One-dimensional model For steady flow with quadratic bottom friction the one-dimensional momentum equation reduces to:

$$\frac{c_{f1}\,|U|U}{d} = F \tag{3.37}$$

where c_{f1} is the friction coefficient for depth-averaged flow. Since U can be assumed positive in steady flow, the expression for the depth averaged velocity becomes:

$$U = \sqrt{\frac{Fd}{c_{f1}}} \tag{3.38}$$

Two-dimensional model Starting point for steady flow with quadratic bottom friction for the two-dimensional model is equation 3.32. The integration constant C_2 is again found by imposing a boundary condition at the bed. The combination of the quadratic boundary condition ($\tau_b = c_{f2}|u_b|u_b$) and equation 3.31 will result in an expression for the velocity at the bed. Substituting this into equation 3.32 gives an expression for C_2 and so the velocity profile becomes:

$$u(z) = \frac{F}{2\nu_t}\left(d^2 - z^2\right) + \sqrt{\frac{Fd}{c_{f2}}} \tag{3.39}$$

where c_{f2} is the friction coefficient for a model that contains information in the vertical direction. Again, integrating over depth gives:

$$\bar{u} = \frac{1}{d}\int_{-d}^{0} u(z)\,\mathrm{d}z = \frac{1}{d}\int_{-d}^{0} \frac{F}{2\nu_t}\left(d^2 - z^2\right) + \sqrt{\frac{Fd}{c_{f2}}}\,\mathrm{d}z = \frac{Fd^2}{3\nu_t} + \sqrt{\frac{Fd}{c_{f2}}} \tag{3.40}$$

Similarly to the linearised case, when assuming $\bar{u} = U$ a relation between c_{f1} and c_{f2} follows:

$$\frac{1}{\sqrt{c_{f1}}} = \frac{1}{\sqrt{c_{f2}}} + \frac{\sqrt{Fd^3}}{3\nu_t} \tag{3.41}$$

with also $c_{f1} \neq c_{f2}$ since the bed shear stress is defined differently.

3.5 Surface elevation

In the preceding section the solutions for the depth-averaged flow velocities, as computed by a one-dimensional and a two-dimensional model respectively, were found. This section discusses the surface elevation as well, which can be included in this analysis via the continuity equation. Recalling the continuity equation from chapter 2:

$$\frac{\partial u}{\partial x} + \frac{\partial v}{\partial y} + \frac{\partial w}{\partial z} = 0 \tag{3.42}$$

The depth-averaged version of the continuity equation is:

$$\frac{\partial \zeta}{\partial t} + d\,\frac{\partial U}{\partial x} = 0 \tag{3.43}$$

where ζ is the surface elevation at the free surface, d is the water depth and U is the depth-averaged velocity. The surface elevation can be found by substituting the expression for the depth-averaged velocity, as computed by the 1D or the 2DV model.

Solution for one-dimensional model

The one-dimensional depth-averaged velocity U previously derived is:

$$U = A \left(\frac{1}{1 - i\sigma_1} \right) e^{i\omega t} \tag{3.44}$$

where $A = F/i\omega$ and $F = -g\,\partial\zeta/\partial x$. Substituting this into the depth-averaged continuity equation (3.43) gives:

$$\frac{\partial \zeta}{\partial t} + d\frac{\partial A}{\partial x}\left(\frac{1}{1 - i\sigma_1} \right) e^{i\omega t} = \frac{\partial \zeta}{\partial t} - \frac{gd}{i\omega}\frac{\partial^2 \zeta}{\partial x^2}\left(\frac{1}{1 - i\sigma_1} \right) e^{i\omega t} = 0 \tag{3.45}$$

Substituting $\zeta(x,t) = \tilde{\zeta}(x)\,e^{i\omega t}$ into equation 3.45 and dividing by $e^{i\omega t}$ gives:

$$i\omega\,\tilde{\zeta} - \frac{gd}{i\omega}\frac{\partial^2 \tilde{\zeta}}{\partial x^2}\left(\frac{1}{1 - i\sigma_1} \right) = 0 \tag{3.46}$$

This differential equation has the following homogeneous solution:

$$\tilde{\zeta}(x) = C_+ e^{-px} + C_- e^{px} \tag{3.47}$$

where

$$\pm p_1 = \pm ik_0\sqrt{1 - i\sigma_1} \tag{3.48a}$$
$$k_0 = \omega/c_0 \quad (= \text{wave number without friction}) \tag{3.48b}$$
$$c_0 = \sqrt{gd} \quad (= \text{wave speed without friction}) \tag{3.48c}$$

The general periodic solution given by equation 3.47 contains two exponentially damped waves propagating in opposite direction. Here $\pm ik_0$ represents the propagation in absence of friction and $\sqrt{1 - i\sigma_1}$ represents the influence of friction. Rewriting p as $p = \mu + ik$:

$$\text{Im}(p) = k_1 = \frac{k_0}{\sqrt{1 - \tan^2 \delta}} \tag{3.49a}$$
$$\text{Re}(p) = \mu_1 = k_1 \tan \delta \tag{3.49b}$$

where $\tan 2\delta \equiv \sigma_1 = \kappa_1/\omega$. Here, instead of working with σ (the ratio of friction to inertia), the so-called "friction angle" δ is defined, as this appears to be more convenient. The general periodic solution of equation 3.47 can be written as:

$$\tilde{\zeta}(x) = C_+ e^{-p_1 x} \qquad\quad + C_- e^{p_1 x} \tag{3.50a}$$
$$\tilde{\zeta}(x) = C_+ e^{-\mu_1 x} e^{-ik_1 x} + C_- 2e^{\mu_1 x} e^{ik_1 x} \tag{3.50b}$$
$$\tilde{\zeta}(x) = \tilde{\zeta}_+ \qquad\qquad + \tilde{\zeta}_- \tag{3.50c}$$

which is just a short-hand notation for the two waves propagating in opposite direction.

Solution for two-dimensional (vertical) model

Similarly, $\bar{u}$ is substituted into the continuity equation, which results in the following complex root:

$$\pm p_2 = \pm ik_0 \left(1 - \frac{\tilde{\gamma}}{bd}\tanh(bd) \right)^{-\frac{1}{2}} \tag{3.51}$$

where

$$\tilde{\gamma} = \left(1 + \frac{i}{\sigma_2\,bd}\tanh\left(bd\right)\right)^{-1} \tag{3.52a}$$

$$\sigma_2 = \kappa_2/\omega \tag{3.52b}$$

$$bd = \sqrt{\frac{i\omega}{\nu_t}}\,d \tag{3.52c}$$

In this case, rewriting p_2 as $p_2 = \mu_2 + ik_2$ requires a tedious amount of algebra, so this is done with the help of Matlab.

The next section illustrates some of the preceding elaborations for a singular progressive wave and waves in a basin closed in one end, for both the one-dimensional and the two-dimensional (vertical) case.

3.6 Examples

3.6.1 Singular progressive wave

For the interpretation of the solution for a singular progressive wave, the time factor is recalled:

$$\zeta(x,t) = \text{Re}\left\{\tilde{\zeta}(x)\,e^{i\omega t}\right\} \tag{3.53}$$

A singular travelling wave is considered, so ζ_+ from equation 3.50c only:

$$\zeta_+(x,t) = \text{Re}\left\{\tilde{\zeta}_+(x)\,e^{i\omega t}\right\} = \text{Re}\left\{C_+\,e^{-px}\,e^{i\omega t}\right\} \tag{3.54}$$

Substituting $p = \mu + ik$ and writing out C_1 in modulus and argument becomes:

$$\zeta_+(x,t) = \text{Re}\left\{|C_+|\,e^{-\mu x}\,e^{i(\omega t - kx + \arg C_+)}\right\} \tag{3.55}$$

or

$$\zeta_+(x,t) = \hat{\zeta}_+(x)\,e^{i(\omega t - kx + \arg C_+)}, \qquad \text{where} \quad \hat{\zeta}_+(x) = |C_+|\,e^{-\mu x} \tag{3.56}$$

This solution shows the surface elevation of a singular progressive wave with k (the imaginary part of p) as the wave number (phase change per unit length). Because the phase varies with x and t via $\omega t - kx$, it concerns a progressive wave in positive x-direction, with phase speed $c = \omega/k$ and $\arg C_+$ is the initial phase (the phase when $\omega t = 0$) of ζ_+ in $x = 0$. The amplitude of $\zeta_+(x,t)$ in $x = 0$ is given by $|C_+|$ and it decreases exponentially in positive x-direction with dampening rate μ.

Two numeric examples are given in table 3.2. Case 1 illustrates a situation in which friction is not very important ($\sigma_1 = 0.05, d = 60$ m); for case 2 friction is more important ($\sigma_1 = 0.5, d = 20$ m). The amplitudes of the surface elevation reduces with a factor $\exp\left(-\mu\Delta x\right)$. Over a distance of $\Delta x = 10$km the one-dimensional reduction factor for case 1 is $\exp\left(-0.015\right) \approx 0.99$ and the two-dimensional is also $\exp\left(-0.015\right) \approx 0.99$. For case 2 the one-dimensional reduction factor is $\exp\left(-0.24\right) \approx 0.78$ and the two-dimensional one is $\exp\left(-0.16\right) \approx 0.86$.

It can be concluded that in some cases there is hardly any difference to be expected between one-dimensional and two-dimensional results. Namely, when friction is of no importance. When friction is important, the model results might deviate strongly.

Table 3.2: *Numeric examples for M_2 with a constant viscosity $\nu_t = 0.05 m^2/s$*

Parameter	Formula	Case 1	Case 2
σ_1		0.05	0.50
σ_2		0.06	0.62
d		60 [m]	20 [m]
c_0	$\sqrt{gd}$	24.3 [m/s]	14.0 [m/s]
k_0	ω/c_0	$5.8 \cdot 10^{-6}$	$1.0 \cdot 10^{-5}$
k_1	$\mathrm{Im}(p_1)$	$5.80 \cdot 10^{-6}$	$1.03 \cdot 10^{-5}$
k_2	$\mathrm{Im}(p_2)$	$5.81 \cdot 10^{-6}$	$8.79 \cdot 10^{-6}$
μ_1	$\mathrm{Re}(p_1)$	$1.45 \cdot 10^{-7}$	$2.44 \cdot 10^{-6}$
μ_2	$\mathrm{Re}(p_2)$	$1.50 \cdot 10^{-7}$	$1.56 \cdot 10^{-6}$

3.6.2 Basin closed in one end

This section treats the case of a rectangular basin with length l that is closed in one end $(x = 0)$, see definition sketch in figure 3.5. Starting point is the general periodic solution given by equation 3.47. To find the integration constants C_+ and C_- boundary conditions are needed. At the closed end $(x = 0)$ $\tilde{u} = 0$, which, via the continuity equation, implies that $C_+ = C_-$. So

$$\tilde{\zeta}(x) = C \cosh(px) \tag{3.57}$$

where C is the new integration constant. At the entrance $(x = l)$ a surface elevation is imposed $\tilde{\zeta} = \tilde{\zeta}_{sea}$, so

$$\tilde{\zeta}(l) = C \cosh(pl) = \tilde{\zeta}_{sea} \quad \Longrightarrow \quad C = \frac{\tilde{\zeta}_{sea}}{\cosh(pl)} \tag{3.58}$$

$$\Longrightarrow \quad \tilde{\zeta}(x) = \tilde{\zeta}_{sea}\frac{\cosh(px)}{\cosh(pl)} \tag{3.59}$$

ũ=0   ζ̃=ζ̃sea
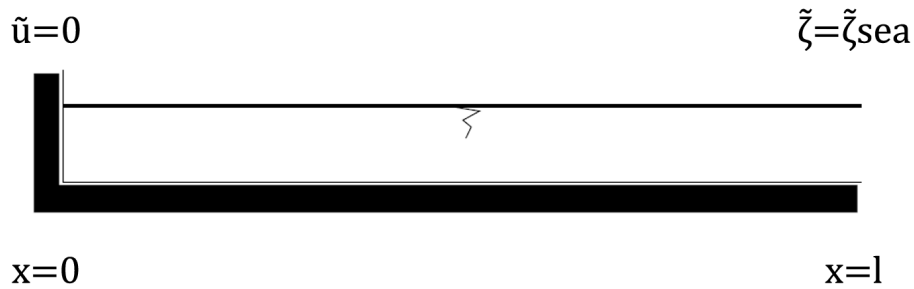
x=0   x=l

Figure 3.5: *Boundary definitions for basin closed in $x = 0$.*

The ratio between the amplitudes at the closed end and the entrance, the amplification factor, is:

$$r = \frac{\hat{\zeta}(0)}{\hat{\zeta}(l)} = \frac{1}{|\cosh(pl)|} \tag{3.60}$$

Because p is different in the one-dimensional case than in the two-dimensional case, the amplification factor differs as well.

3.7 Discussion

In addition to the findings of the previous chapter, the preceding analytical approach confirmed the importance of the eddy viscosity ν_t, the frequency ω and the water depth d. Analytical solutions to a depth-averaged (1D) model and a model that does contain information in the vertical (2DV) are:

$$1D: \quad U = \tilde{A} \cdot \left(\frac{1}{1 - i\sigma_1} \right) e^{i\omega t}$$

$$2DV: \quad \bar{u} = \tilde{A} \cdot \left(1 - \frac{\tilde{\gamma}}{bd} \tanh(bd) \right) e^{i\omega t}$$

where $\tilde{\gamma}$ is a function of σ_2 and bd only. So, the depth-averaged velocities in both models are very similar-looking and may be described by a function of the dimensionless σ_1-parameter or the dimensionless σ_2-parameter and the dimensionless bd-parameter, respectively, where

$$\sigma_1 = \frac{8}{3\pi} c_{f1} \frac{\hat{U}}{\omega d}$$

$$\sigma_2 = \frac{8}{3\pi} c_{f2} \frac{\hat{u}_b}{\omega d} \quad \text{and} \quad bd = \sqrt{\frac{i\omega d^2}{\nu_t}}$$

To connect the above solutions, the choice was made to assume the depth-averaged velocities of both cases to be equal for steady flow. This assumption appears to be very effective for the objective of this chapter.

Concentrating on the propagation of one single predominant tidal constituent (M_2), the analytical approach in this chapter shows that certain conditions may cause significant differences between depth-averaged velocities, as computed by a two-dimensional and a three-dimensional model respectively. However, thorough research resulted in the conclusion that it is reasonably hard to find such conditions in practice. Therefore, in combination with the uncertainties around the connecting relation between the two models, the figures showing amplitude and phase ratios should be treated with care. Roughly, the largest differences are to be expected at locations with reasonable water depth ($d > 60$ m) and high velocities ($\hat{U} > 1$ m/s). Also, it is noticed that the amplitude ratio is practically always > 1, and the phase ratio < 1 for shelf seas.

The analytical solutions were found by linearising the equations, which has its limitations obviously. Distinction is made between two sorts of non-linear effects:

1. Non-linearities caused by higher-order terms in the equations of motion, i.e. advective acceleration and friction terms. The linearisation of the friction term κU is based on optimal reproduction of the predominant tidal constituent. While effective for the objective of this research, such linearisation distorts propagation and generation of other tidal constituents, including the residual current. Therefore, in the next chapter it should be assured that advection plays no role.

2. Non-linear effects caused by geometrical non-linearities that are the results of the cross section depending on the surface elevation ζ. This comes into play with varying water depths and storage width for instance, which will be important when modelling a continental shelf sea (chapter 5).

Chapter 4

Numerical modelling: conceptual simulations

In the previous chapter analytical solutions were found for strongly simplified equations of motion neglecting Coriolis, advection, density differences and wind stress. While adopting a linear approach to determine the bottom friction, this provided insight into the difference between a depth-averaged model and one with vertical information (using a constant vertical eddy viscosity). In order to find the effect of averaging over the water depth on numerical results, this chapter tries to extend the analytical findings from the previous chapter by testing the same approach for numerical modelling.

When simulating a shelf sea or estuary, generally many factors are incorporated, which makes it ambiguous to isolate the processes that matter for this research. So, before studying an actual case of modelling a continental shelf sea (which is done in the next chapter) this chapter treats several test cases for schematized rectangular basins.

Section 4.1 gives a technical introduction of the used numerical flow models, FINEL2D and FINEL3D. Section 4.2 presents the model set-up for this chapter. Section 4.3 treats a numerical example for steady flow and section 4.4 for unsteady flow.

4.1 FINEL2D/3D

The computational models applied in this study are the implicit two-dimensional and implicit three-dimensional version of the finite element model FINEL. These models, FINEL2D and FINEL3D, solve the two-dimensional Shallow-Water Equations (section 4.1.1) and the complete three-dimensional Navier-Stokes equations respectively, using an unstructured computational mesh of triangles (2D) or tetrahedrons (3D). The use of an unstructured grid enables the user to treat complex flow geometries in a relatively straightforward way.

The acronym FINEL stands for FINite ELements, referring to the solution method: the finite element method (FEM). FEM is a discretization technique for partial differential equations. Many different discretization techniques exist. Some well-known classes are listed below (Labeur, 2009).

- *Finite difference methods* use a mapping of the flow domain onto a regular grid of discrete points. The flow variables are represented by point-wise values on an associated set of grid points while the differential equations that determine the time evolution of these variables are approximated from Taylor-series expansions between the discrete data points.

- *Finite volume methods* are based on a partitioning of the flow domain into a number of control volumes or cells each representing a local flow state. Balance equations are used to determine the rate of change of the flow state within each volume. This requires the determination of fluxes between control volumes from the cell based data.

- *Spectral methods* use a set of analytical global basis functions covering the entire domain to represent the flow variables. Traditionally, goniometric or polynomial functions are used for this purpose. Substitution into the differential equations directly yields analytical expressions from which the evolution of the flow field is evaluated. In case of non-linear problems this procedure requires an orthogonal projection of the analytical solution onto the basis functions.

- *Finite element methods* finally, also use a set of basis functions to represent the flow field. However, the basis functions are not defined globally but locally using partitions of the domain called elements. The governing equations are approximated using weak formulations. This only requires square integrability of functions and their derivatives which allows rather simple classes of basis functions and elements of more or less arbitrary size and shape.

The main advantage of the finite element method over the other methods is that it is well suited to be applied on irregular domains. However, a drawback of the method is that the matrix structure of finite element problems is not as nicely ordered as finite volume and finite difference techniques do.

The numerical heart of FINEL3D is based on the three-dimensional implicit finite element model FINLAB, which has been developed by Labeur (2009), see also Labeur and Wells (2012). The code FINEL3D has been developed by Svašek Hydraulics, combining the mathematical concepts of FINLAB with specific input-output routines for use within civil engineering projects. The implicit model FINEL2D is basically a spin-off from FINEL3D, to which the numerical concepts of FINLAB have been applied in a depth-averaged fashion. A brief overview of relevant numerical aspects of the 2D and 3D model is given here.

4.1.1 Governing equations

The depth-integrated shallow water equations are the basis of the flow module of FINEL2D, see for example Vreugdenhil (1994) for an overview. The continuity equation reads:

$$\frac{\partial \zeta}{\partial t} + \frac{\partial (HU)}{\partial x} + \frac{\partial (HV)}{\partial y} = 0 \tag{4.1}$$

where $H = \zeta + d$. In fact, this is equation 2.1 integrated over depth. The depth-integrated momentum balances are derived from equations 2.2 a and b, which results in x-direction in:

$$\frac{\partial (HU)}{\partial t} + \frac{\partial (HU^2)}{\partial x} + \frac{\partial (HUV)}{\partial y} - HfV + gH\frac{\partial \zeta}{\partial x} - \frac{1}{\rho_0}\left(\tau_{x,b} + \tau_{x,w} + \tau_{x,r}\right) = 0 \tag{4.2}$$

where $\tau_{x,b}$ is the bed shear stress, $\tau_{x,w}$ is the wind shear stress and $\tau_{x,r}$ is the radiation stress due to surface waves. The momentum balance in y-direction reads:

$$\frac{\partial (HV)}{\partial t} + \frac{\partial (HUV)}{\partial x} + \frac{\partial (HU^2)}{\partial y} + HfU + gH\frac{\partial \zeta}{\partial y} - \frac{1}{\rho_0}\left(\tau_{y,b} + \tau_{y,w} + \tau_{y,r}\right) = 0 \tag{4.3}$$

So, in addition to bottom shear stress and barotropic pressure gradients that were discussed in the previous chapter, the effect of advection must also be considered. Moreover, external forces like the Coriolis force, wind shear stress and radiation stress due to surface waves can be taken into account. Though, this will not be used for this thesis.

4.1.2 Solution method

The discretization of FINEL2D/3D is based on a combination of the Continuous Galerkin (CG) and Discontinuous Galerkin (DG) approaches within the finite element method. Linear continuous elements are used for approximating the pressure (or the piezometric level), and discontinuous linear elements are applied for the velocity components. These elements are either triangles (2D) or tetrahedrons (3D); their degrees of freedom are located at element nodes. Usually, DG methods have much more degrees of freedom than CG methods. Consequently, DG problems do take much more computational time to be solved. Within FINEL, CG and DG techniques have been blended into a new approach coined Galerkin Interface Stabilization (GIS, (Labeur, 2009)), in order to obtain the accuracy of DG methods combined with the computational speed of CG methods. The global system of linear equations has the same size as that of a CG method (global degrees of freedom on the nodes only), which makes the model rather compact and quick to solve.

Discretization in time is established with the well-known implicit θ-method (which can be made fully implicit for $\theta = 1$, or second-order accurate for $\theta = 0.5$). For FINEL2D both an explicit and an implicit version are available, but FINEL3D only comes in implicit version. To accommodate an accurate comparison between FINEL2D and FINEL3D, the implicit version of FINEL2D will be used for this thesis. An implicit scheme means that the equation for the variable in the new time step u^{n+1} is coupled to both the terms u^{n+1} and u^n. Thus each new time step requires the solution of a system of coupled equations. In FINEL2D/3D each global system of linear equations is solved using the iterative matrix solver BiCGSTAB with efficient pre-conditioning. The resulting numerical implementation has second-order accuracy in space and first-order or second-order accuracy in time, dependent on the chosen value of θ. By the GIS approach, the momentum advection terms are effectively stabilized without the need for additional artificial diffusion.

4.1.3 Turbulence modelling

Turbulence modelling involves the computation of the net contribution of turbulent fluctuations to the mean flow. To this end, the underlying momentum equations are averaged over a time interval much larger than the turbulence time-scale to yield the Reynolds Averaged Navier-Stokes (RANS) equations, as discussed in 2.2. This paragraph explained that the averaging procedure leads to a closure problem which requires a turbulence model. The mean turbulent stress can be modelled in terms of the gradient of the resolved velocities, analogous to the representation of viscous stresses. The turbulent viscosity expresses the transport of momentum in a turbulent flow. In FINEL3D several models for this turbulent viscosity are available:

- constant eddy viscosity (in m^2/s);

- Prandtl mixing-length model;

- $k - \epsilon$ model;

- Large Eddy Simulation (Smagorinsky-subgrid model).

The constant eddy viscosity model is a simple model prescribing the eddy viscosity as the product of a velocity and a length scale, as was used in chapter 2 and 3 ($\nu_t = \frac{1}{6}\kappa d u_\star$). The Prandtl mixing-length model uses the *mixing length hypothesis* in which the velocity that characterizes the turbulent fluctuations is proportional to the velocity difference in the mean flow over a distance l_m over which the mixing or transport of momentum takes place, and is given by: $l_m \cdot \partial \bar{u}/\partial z$. By using l_m again as the governing length scale, the eddy viscosity can be written as the product of this length scale squared and the local velocity gradient and is described by a so-called *Bakhmetev*-profile. The $k - \epsilon$ model relates the turbulence viscosity to

the turbulence kinetic energy k and the turbulence dissipation rate ϵ. The evolution of k and ϵ in time is described by transport equations (Nieuwstadt, 1992). If large, coherent turbulent structures are to be resolved, the Large Eddy Simulation (LES) approach should be used. In LES models larger turbulent scales are directly resolved on the computational grid, whereas smaller (sub-grid) scales are accounted for by a closure formulation.

The latter two turbulence models are beyond the scope of this thesis. The constant eddy viscosity model will be the starting point for this chapter as a continuation of the preceding chapters. This chapter is divided in two sections on steady and unsteady flow, respectively. Both sections first treat simulations with the constant eddy viscosity model in combination with linearised bottom friction. Next, when modelling with quadratic bottom friction, both constant eddy viscosity model and the mixing-length model are studied.

4.1.4   Boundary conditions

FINEL2D/3D have a variety of boundary conditions to close and solve flow problems. The simulations of this chapter are done with (a combination of) the following options:

- closed boundaries at the bottom, bank or wall (with or without wall friction);

- free surface boundary;

- constant water levels on open boundaries;

- harmonically varying water levels.

The bottom boundary condition will now be discussed in more detail.

Bottom boundary condition

In Chapter 3 section 3.4.2 it was found that the friction coefficient in a depth-averaged model (c_{f1}) was different from the one in the model with vertical information (c_{f2}), while a constant vertical eddy viscosity was used. Numerical modelling in practice commonly uses a viscosity that is vertically varying in accordance with the turbulence mixing-length model (Bakhmetev-model). Substitution of this definition of the eddy viscosity into equation 3.30 and integration over the water depth delivers the well-known logarithmic velocity profile:

$$u(z) = \frac{u_\star}{\kappa} \ln \left(\frac{z + d}{z_0} \right) \tag{4.4}$$

where $u_\star$ is the shear stress velocity, κ is the Von Karman constant (not to be confused with the bottom friction coefficients κ_1 and κ_2). The parameter z_0 can be linked to the actual roughness; for rough walls Nikuradse (1933) found:

$$z_0 = \frac{k_N}{30} \tag{4.5}$$

where k_N is known as the Nikuradse roughness height, which has been determined experimentally.

Analogous to section 3.2 for a depth-averaged model the bed shear stress can be related to the depth-averaged velocity via $\tau_b = c_{f1}|U|U = u_\star^2$. In combination with the logarithmic profile of equation 4.4 an expression for the friction coefficient c_{f1} is found:

$$\frac{1}{\sqrt{c_{f1}}} = \frac{1}{\kappa} \ln \left(e^{-1} \frac{d}{z_0} \right) \tag{4.6}$$

Analogous to section 3.3 for a model with a vertical dimension the bed shear stress can be related to the bottom current u_b with a friction coefficient (c_{f2}) via $\tau_b = c_{f2}|u_b|u_b$. The velocity component u_b is located in the first layer just above the bed. Yet, it is fairly arbitrary which velocity is chosen to be "the" bottom current. For a staggered grid, as is the case for Delft3D, the Delft3D Flow Manual (Deltares, 2013) assumes the first grid point above the bed to be situated in the logarithmic boundary layer. Let Δz_b be the distance to the computational grid point closed to the bed, so u_b is located half way of the computational bed layer. The WAQUA/TRIWAQ Manual (Rijkswaterstaat, 2012) presents a similar method.

FINEL3D is based on a co-located grid, which means that all variables are located at the same physical point. So, u_b is located exactly at the bottom, which results in a problem. Namely, according to the logarithmic profile u_b at the bottom would be minus infinity, which is practically impossible. Therefore, it seems impossible to determine the bed shear stress from u_b. The answer to this problem is found in the formulation of the bottom stress defined as:

$$\tau_b = |u_\star|u_\star \quad \implies \quad u_b = \frac{u_\star}{\sqrt{c_{f2}}} \tag{4.7}$$

This estimate for u_b is used to determine the velocity gradient in the bed layer that, in combination with the Bakhmetev *mixing-length hypothesis* (see section 4.1.3) delivers a shear stress that has to be equal to the bottom shear stress defined above. This will result in an expression for the friction coefficient c_{f2}:

$$\frac{1}{\sqrt{c_{f2}}} = \frac{1}{\kappa} \ln \left(e^{-2} \frac{\Delta z_b}{z_0} \right) \tag{4.8}$$

Often detailed 3D calculations are preceded by orienting depth-averaged calculations. Then, the depth-averaged coefficient c_{f1} may be used for calibration of the 3D model and therefore a relation between c_{f1} and c_{f2} is needed. The relation between c_{f1} and c_{f2} for a Bakhmetev profile for the vertical eddy viscosity is found by equating 4.6 and 4.8:

$$\frac{1}{\sqrt{c_{f1}}} = \frac{1}{\sqrt{c_{f2}}} - \frac{1}{\kappa} \ln \left(\frac{e^{-1}\Delta z_b}{d} \right) \tag{4.9}$$

Converting rule for constant vertical eddy viscosity

The relation between c_{f1} and c_{f2} for a *constant* vertical eddy viscosity is expressed in equation 3.41 and for a *Bakhmetev* viscosity profile equation 4.9 can be used. Equating these two expressions results in a calibration rule to accommodate similar numerical simulations with either a constant vertical eddy viscosity or a Bakhmetev-profile. Solving:

$$\frac{\sqrt{Fd^3}}{3\nu_t} = -\frac{1}{\kappa} \ln \left(\frac{e^{-1}\Delta z_b}{d} \right) \tag{4.10}$$

gives:

$$\nu_t = \frac{\kappa u_\star d}{3 + 3\ln(nz)} \tag{4.11}$$

where nz is the number of layers in the vertical. Applying this rule will result in approximately the depth-averaged velocity for a flow problem regardless of what turbulence model is used: constant eddy viscosity or Bakhmetev.

4.2 Model set-up

Similarly to what is done to get to the analytical solutions of Chapter 3, the numerical examples of this chapter solve equation 3.2 by forcing a water level gradient (which is notated as F, the right hand side of this equation). The computations are performed for steady flow and unsteady,

periodic flow. In the steady case the water level gradient is constant in time (section 4.3). In the unsteady case periodically varying flow is studied (section 4.4). In both cases, first, the numerical simulations are done with linearised bottom friction corresponding to the analytical approach. The numerical response of the (depth-averaged) horizontal velocities, should ideally correspond to the analytical velocity profiles averaged over depth. The observed difference can only be caused by the numerical approximations, i.e. time integration and (horizontal) discretization. When it is checked that the numerical and analytical results match nicely, it is desirable to bring back FINEL to its original settings: with the quadratic formulation of the bottom friction term. Subsequently, more complex cases can be studied, which is a important advantage of the computer model over the analytical approach. It enables the linearisation to be dropped, which brings FINEL back to its original code used in civil engineering practice, to see if the analytical approach still holds in that case.

Both FINEL2D and FINEL3D use the same grid, which is extended in vertical direction with an arbitrary number of vertical grid points for FINEL3D. The computational mesh for both models is commonly generated using Google Earth, various MATLAB routines and the grid generator TRIANGLE.

For both flow cases (section 4.3 and 4.4) the model is set up as a rectangular basin with two open boundaries at the short sides and a water depth of 60 m. The width of the basins (200 m) is small compared to the length, since there is no interest in lateral variations in these conceptual simulations. For the *steady* flow case (section 4.3) the basin is elongated to a length of 100 km. This length L_{basin} is relatively long because it is needed for the water level gradient to fully develop. The purpose of the *unsteady* flow case (section 4.4) essentially is to study the instantaneous response in the same way as was done in Chapter 3. Therefore $L_{basin} = 1000$ m, which is short to avoid phase lags within the model domain. Figure 4.1 shows the mesh for a maximum surface area of the elements of 5000 m^2 used for section 4.3 to simulate steady flow; figure 4.2 shows the mesh for a maximum mesh size of 5000 m^2 used for 4.4 simulating unsteady flow. Unstructured grids are used in agreement with the case study of the next chapter because it simulates normal circumstances that model user deal with in practice. Also, this way grid dependencies are more easily observed, if present.
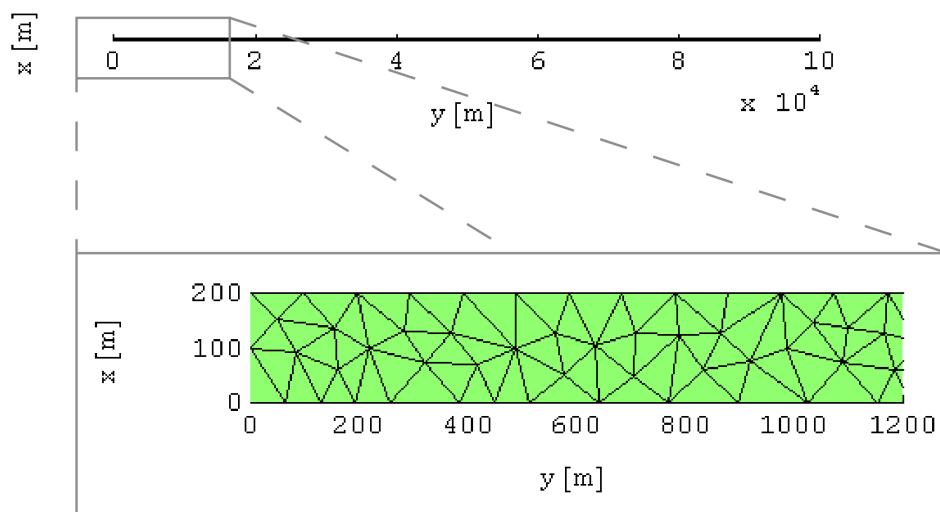

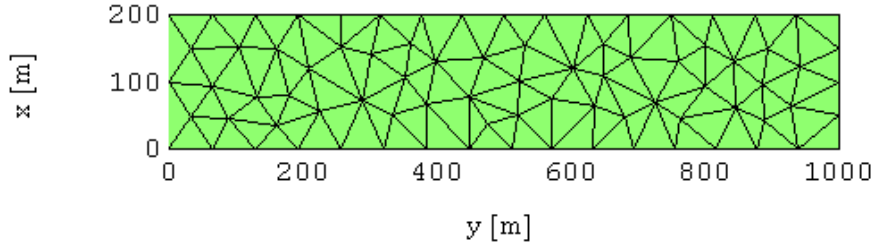Figure 4.1: *Mesh for a long channel used for section 4.3 Steady flow.*

Figure 4.2: *Mesh for a short rectangular basin used for section 4.4 Unsteady flow.*

First, some testing was done in order to find a suitable time step, vertical discretization and horizontal eddy viscosity. Next, it was checked that the solution for the 2DH and the 3D model gave exactly the same output in a frictionless case.

4.3 Steady flow

The boundary conditions for the steady case specify a water level of 1 m on the inflow boundary (left), a water level of 0 m on the outflow boundary (right), and a zero normal velocity on the side-walls and the surface (upper boundary), see figure 4.3. In this way, the water level is fixed at a gradient of $i_w = 10^{-5}$. Physically, it would have been better to give the bottom the same slope, but for these simulations the bottom is flat.
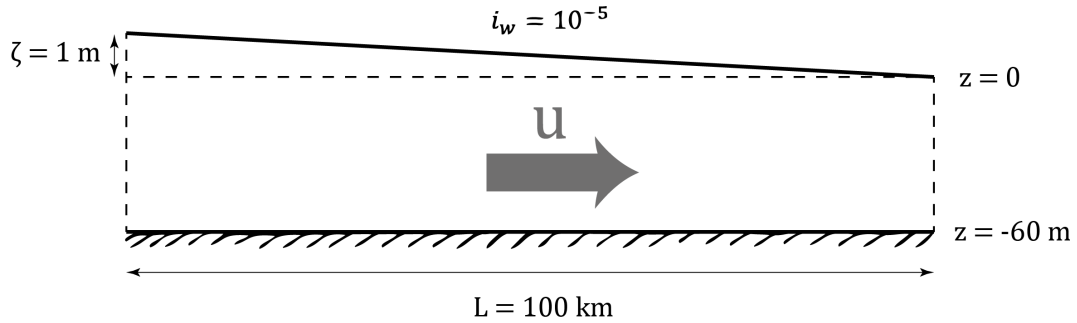

Figure 4.3: *Steady flow in a long channel.*

When 3D results are averaged over depth, they can be straightforwardly compared to corresponding results from the 2D model. The question rises how to calibrate the models so that they describe exactly the same steady flow problem. The formulations of the bottom friction should be consistent with each other. As this study treats linear and quadratic formulations of the bottom friction, is it easy to get lost in this matter. For this chapter, it is found reasonable to choose the same value for the Nikuradse roughness k_N in both models, since this parameter has a dimension of length regardless of the model domain. The value of $z_0 = k_N/30$ will then be constant as well.

In fact, c_{f1} was chosen to be 0.002 and with this value it was calculated that k_N should be 0.086 m en therefore c_{f2} should be 0.0042. With these values the first simulation was performed for the case with quadratic bottom friction. Subsequently, the linearised friction coefficients, κ_1 and κ_2, can be determined with values for the velocity $|U|$ and $|u_b|$ from the simulation (see

table 4.1 for their values):

$$\kappa_1 = c_{f1} \frac{|U|}{d} \tag{4.12a}$$

$$\kappa_2 = c_{f2} \frac{|u_b|}{d} \tag{4.12b}$$

This is the input for the model with linearised bottom friction. So, the simulation with quadratic bottom friction was actually performed in advance of the linearised case. This enables a comparison between all simulations (2D and 3D, linear and quadratic).

In combination with quadratic bottom friction two turbulence models are studied: the constant eddy viscosity and the Prandtl mixing-length model. In the end, both computations will result in the same depth-averaged velocity as long as a specific value is chosen for the vertical eddy viscosity, corresponding with the specific bottom friction coefficients that were chosen. This is guaranteed by using the calibration rule from equation 4.11 resulting in $\nu_t = 0.22$ m^2/s.

Table 4.1: *Input parameters for the steady flow case.*

Parameter	Calculated value
c_{f1}	0.002
c_{f1}	0.004
κ_1	$5.7 \cdot 10^{-5}$
κ_2	$8.3 \cdot 10^{-5}$
ν_t	0.22 m^2/s

4.3.1 Linearised bottom friction

Firstly, simulations are done for the long channel of figure 4.1 with linearised bottom friction. The values of the input parameters used for these simulations are summarised in table 4.2. The theoretical velocity profiles for steady flow with linearised bottom friction were derived in chapter 3, given by equations 3.33 and 3.34. These profiles are used to compare the numerical results with. Unlike the analytical solutions, do the numerical simulations have slight longitudinal variation. The velocity profile at the end of the channel ($y = 100$ km, see figure 4.1) is assumed to be fully developed, so this point is studied in more detail.

Table 4.2: *Input parameters for the steady case with linearised bottom friction.*

Fundamental parameters	Derived parameters
$g = 9.81$ m/s^2	$z_0 = k_N/30$ m
$i_w = 10^{-5}$	$\Delta z_b = d/nz = 10$ m
$d = 60$ m	$\kappa_1 = 5.7 \cdot 10^{-5}$
$k_N = 0.086$ m	$\kappa_2 = 8.3 \cdot 10^{-5}$
$nz = 6$	$\nu_t = 0.22$ m^2/s

As expected, both the 2D and 3D numerical results are in agreement with the analytical solutions. When plotting the FINEL3D velocity profile $u(z)$ over the water depth, it shows perfect correspondence with the theoretical parabolic profile (see figure 4.4, in red the FINEL3D result and in black the analytical solution). Also, averaging the numerical 3D profile over depth resulting in $\bar{u}$, has practically the same value as U from FINEL2D (blue dashed line).
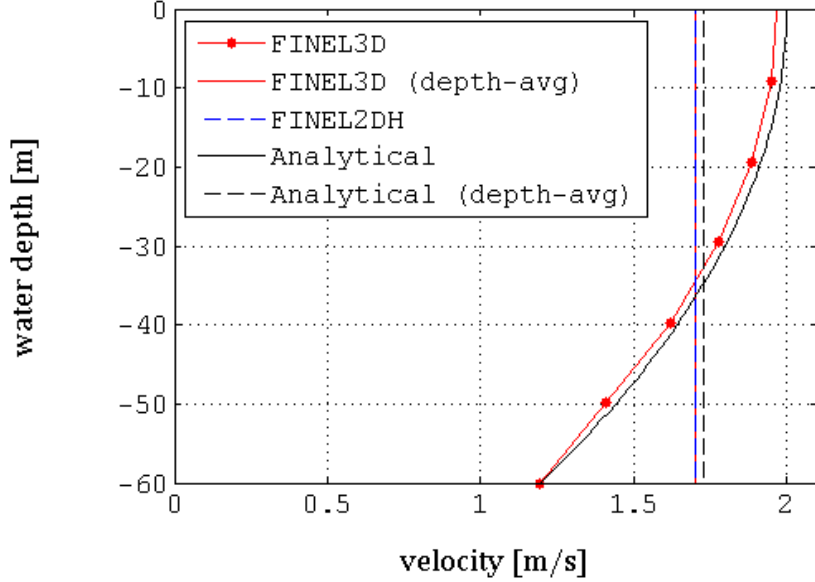

Figure 4.4: *Parabolic velocity profiles for steady flow with linearised bottom friction and constant vertical eddy viscosity.*

4.3.2   Quadratic bottom friction

Next, an example that investigates the influence of the linearisation on the numerical solution, in comparison with analytical profiles, for the same long channel of figure 4.1. For this example, the original FINEL models are used calculating the bottom friction with a quadratic formulation. First, the simulations are done with a constant eddy viscosity and subsequently another turbulence model is tested, the Bakhmetev mixing length model. The values of the input parameters used for these simulations are summarised in table 4.3.

Table 4.3: *Input parameters for the steady case with quadratic bottom friction.*

Fundamental parameters	Derived parameters
$g = 9.81$ m/s^2	$z_0 = k_N/30$ m
$i_w = 10^{-5}$	$\Delta z_b = d/nz = 10$ m
$d = 60$ m	$c_{f1} = 0.002$
$k_N = 0.086$ m	$c_{f2} = 0.0042$
$nz = 6$	$\nu_t = 0.22$ m^2/s
$\kappa = 0.4$	$u_\star = 0.077$ m/s

Analogous to the linearised case, the numerical results are compared to the theoretical velocity profile. The theoretical velocity profile for steady flow with quadratic bottom friction is described by equations 3.39 and 3.40.

Again, the numerical results completely agree with the analytical solution as is shown in figure 4.5 for the case with constant eddy viscosity, and in figure 4.6 for the case with the Bakhmetev mixing length model. The velocity profiles are reproduced correctly; in the case of constant eddy viscosity a parabolic velocity profile and in case of the Bakhmetev model the logarithmic profile. Both 2D and 3D simulations match the theory perfectly.
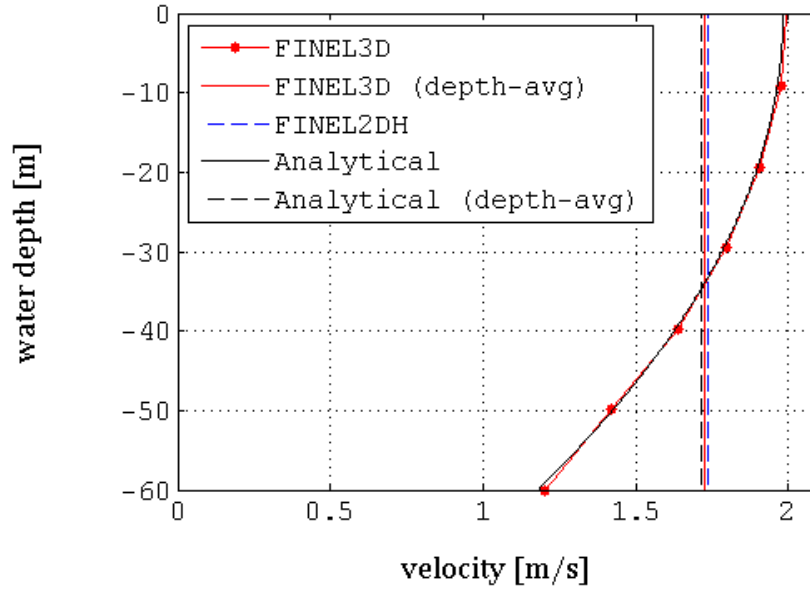

Figure 4.5: *Parabolic velocity profiles for steady flow with quadratic bottom friction and constant vertical eddy viscosity.*
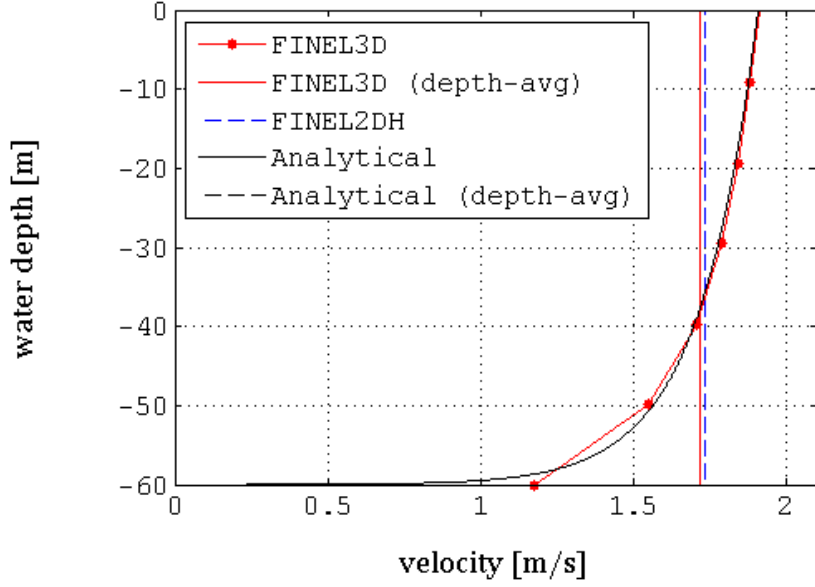
Figure 4.6: *Logarithmic velocity profiles for steady flow with quadratic bottom friction and viscosity defined by the Bakhmetev model.*

4.3.3   Discussion

Both for a linearised and a quadratic formulation of the bottom friction it is shown that the numerical results for this steady flow case show great similarity with the analytical solutions, as expected. As the surface elevation is much smaller than the water depth advection can be neglected so that the numerical response is reproduced in perfect agreement with the theory, providing a good starting point for unsteady flow.

4.4   Unsteady flow

Real environmental flows are often unsteady, as for example the reversing flow in a tidal estuary or the wind-driven flow in a lake caused by a passing storm. By imposing two water levels at the open boundaries ($y = 0$ and $y = 1000$ m in figure 4.2) that are equal in amplitude but slightly differ in phase, a periodically varying water level gradient is obtained (see figure 4.7). Then, this water level gradient is the driving force in the basin in agreement with the analytical approach of the previous chapter. This basin is chosen relatively short so that damping is insignificant. The phase difference α is calculated in table 4.4.

Table 4.4: *Unsteady flow parameters.*

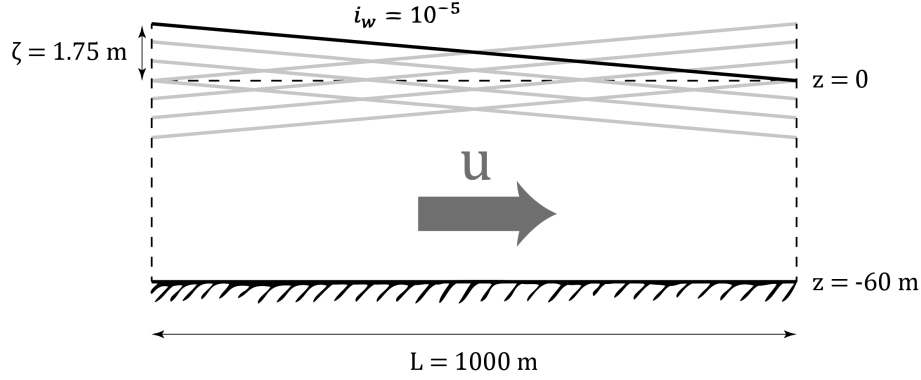| Fundamental parameters	Derived parameters
$g = 9.81$ m/s^2	$c = \sqrt{gd} \approx 24$ m/s
$d = 60$ m	$L_{wave} = cT \approx 10^6$ m
$T = 44700$ s	$\Delta L_{wave} = L_{basin}/L_{wave}$
$L_{basin} = 10^3$ m	$\alpha = \Delta L_{wave} \cdot 2\pi \approx 0.0058$ rad

Figure 4.7: *Unsteady flow in a short basin.*

Other than the analytical approach, do these simulations have some longitudinal variation. The velocity profile in the middle of the channel ($y = 500$ m in figure 4.2) is very similar to the mean velocity profile (in longitudinal direction), so this location is studied in more detail. The time series of the flow velocity are plotted for both the analytical and the numerical results, as computed by the linear and the quadratic version of FINEL2D and FINEL3D in figure 4.8. This figure shows for two days (in which almost 4 tidal cycles fit) that both the 2D and 3D numerical signals perfectly match with the theory. Moreover, it can be seen that the quadratic bottom friction apparently has a limited effect on the flow velocity for this case.
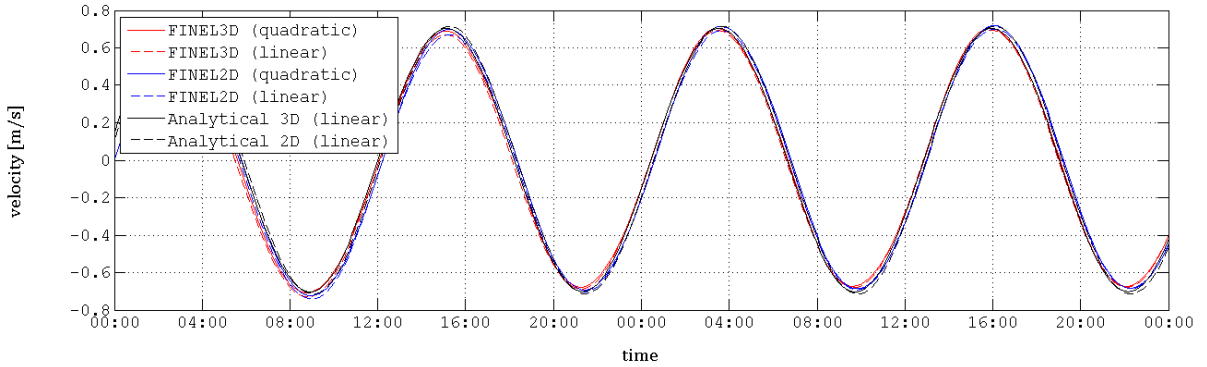

Figure 4.8: *Time series for unsteady flow (averaged over depth) calculated with a constant vertical eddy viscosity and both linearised and quadratic bottom friction.*

Likewise, plotting the FINEL3D velocity profile $u(z)$ over the water depth shows good correspondence with the analytical parabolic profile (see figure 4.9). Averaging the numerical three-dimensional velocity profile over depth gives $\bar{u}$, which will be compared to U computed by FINEL2D for the linearised and the quadratic case. In general, the velocity as computed by the two-dimensional model is slightly higher than the depth-averaged velocity as computed by the three-dimensional model. For the analytical profiles the observed amplitude ratio is:

$$\frac{U_{2D}}{U_{3D}} = \frac{0.714}{0.699} \approx 1.02 \tag{4.13}$$

Apparently, for the conditions that were chosen here the three-dimensional effects are not expected to be very important. The conditions were chosen because they correspond to realistic shelf sea conditions.
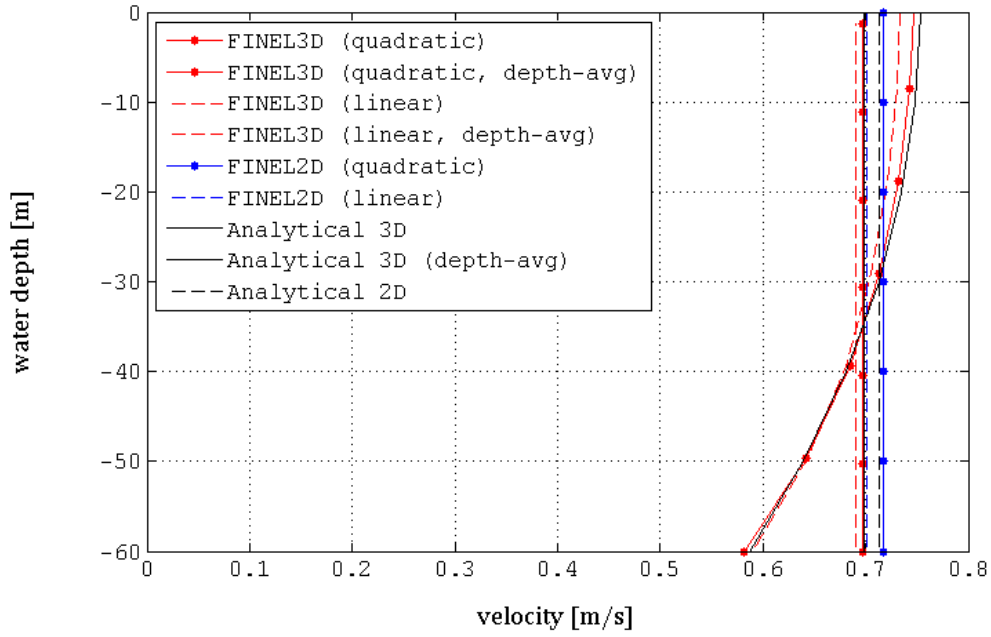
Figure 4.9: *Velocity profiles for unsteady flow calculated with a constant vertical eddy viscosity and both linearised and quadratic bottom friction.*

4.4.1 Linearised bottom friction

The velocity amplitude ratio for the numerical profiles with linearised bottom friction is:

$$\frac{U_{2D}}{U_{3D}} = \frac{0.701}{0.691} \approx 1.01 \tag{4.14}$$

4.4.2 Quadratic bottom friction

The velocity amplitude ratio for the numerical profiles with quadratic bottom friction is:

$$\frac{U_{2D}}{U_{3D}} = \frac{0.715}{0.697} \approx 1.03 \tag{4.15}$$

4.4.3 Discussion

The numerical results for unsteady flow show good correspondence with the theory. Analogous to the findings of the previous chapter, where the importance of the eddy viscosity ν_t, the frequency ω and the water depth d was discussed, the $\omega d^2/\nu_t$-parameter and the σ-parameters can be calculated. In this case, $U \approx 0.70$ m/s and $u_b \approx 0.59$ m/s, so that

$$\frac{\omega d^2}{\nu_t} = 2.30$$

$$\sigma_1 = \frac{8}{3\pi} c_{f1} \frac{\hat{U}}{\omega d} \approx 0.14$$

$$\sigma_2 = \frac{8}{3\pi} c_{f2} \frac{\hat{u}_b}{\omega d} \approx 0.25$$

While there is a significant difference between the two σ-values, the absolute values are reasonably low. Low σ-values confirm that bottom friction is rather unimportant compared to inertia, which explains the linear behaviour in figure 4.8.

Also, the analytical approach revealed that the velocity as computed by the 2D model is in more likely to be larger than the 3D velocity than vice versa. This behaviour is certainly recognised in the above numerical examples as all the calculated ratio are > 1.

4.5   Conclusions

The numerical examples in this chapter show perfect correspondence to the analytical solutions of the previous chapter. No significant differences between the 2D and 3D results were observed because the conditions were chosen such that the bottom friction is of less importance compared to inertia. In the previous chapter it was already concluded that it is reasonably hard to find extreme conditions that are realistic in practice. However, the next chapter will show that they certainly exist.

Chapter 5

Numerical modelling: in practice

To provide an example of the practical application of the previously found theoretical profiles and numerical behaviour, this chapter studies an actual case. In the previous chapter it was found that the numerical results as computed by a two-dimensional and a three-dimensional flow model show excellent similarities for simple geometries; both with each other as with analytical solutions. This was expected to be the case, since all input was equal and converted similarly, so that the only differences could be caused by the numerical discretization in space and time. For the schematized rectangular basins these differences were nihil. This chapter will further examine the numerical behaviour for more complex and more realistic simulations. As the development of this study is motivated by practical problems in the North Sea, its implementation is tested using the European Continental Shelf Model.

Section 5.1 gives an overview of the model domain of this European Continental Shelf Model and the computational grid applied. Section 5.2 will elaborate on the properties of the numerical model for the specific case studied in this chapter, the applied boundary conditions and other parameters that were put in. In 5.3 the analytical approach of Chapter 3 is applied onto the ECSM as an example application in practice. Finally, section 5.4 discusses the numerical model results.

5.1   European Continental Shelf Model (ECSM)

Shelf seas can conveniently be considered to extend from just below the low tide level at the coastline (the baseline) out to the shelf break, as stated in Chapter 1. Most are bounded on one side by land and on the other by open ocean, but some, such as the North Sea, are semi-enclosed. The North Sea is located on the North-Western part of the European Continental Shelf. For this chapter FINEL2D and FINEL3D are applied onto the so-called European Continental Shelf Model (ECSM), of which the outlines are shown in figure 5.1. This model is an existing model used and developed by Svašek Hydraulics.

Figure 5.1: *Outlines and history points for ECSM model.*

The model domain of the ECSM model is fairly large. The model boundaries follow a large part of the North-West European coasts, and the boundaries facing the ocean are all located at the shelf break to the Atlantic Ocean. The computational mesh is shown in figure 5.2 where the color illustrates the bathymetry. The southern part of the North Sea, off the coasts of The Netherlands, Denmark and the southern part of the UK, typical water depth are $\approx 30 - 50$ m. Shifting further offshore, towards Scotland and Norway, the water depth increases to values of ≈ 100 m. At the model boundaries, the shelf break, the water depth reaches typically a value of ≈ 200 m. An exceptional region in this matter is located off the coast of Norway where water depths are > 600 m, the so-called Norwegian Trench. Figure 5.2 shows the computational grid applied on the ECSM model; in color the bathymetry. This figure zooms in on the Orkney Islands, an archipelago in Northern Scotland, to show the mesh in more detail.
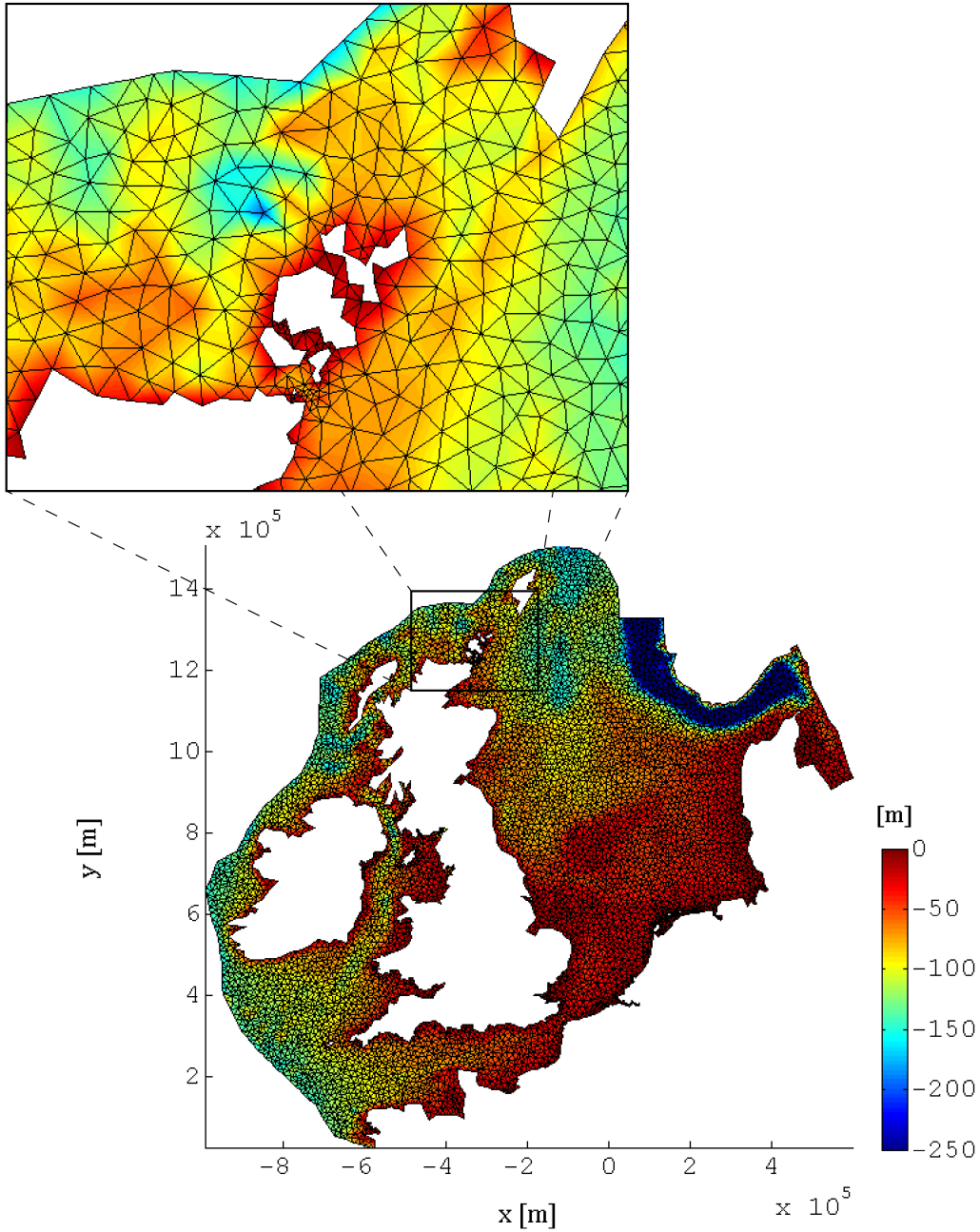
Figure 5.2: *Computational mesh for the Europian Continental Shelf Model.*

5.2 Model set-up

Coriolis

Due to the rotation of the earth, the flow is deflected to the right on the Northern Hemisphere. The influence of earth's rotation on the flow direction, is in the momentum equations captured by the Coriolis terms, were neglected in the preceding chapters. Since the Coriolis terms depend on latitude, they are taken into account in this large-scale model. The Coriolis parameter is given by:

$$f = 2\Omega \sin(\phi) \tag{5.1}$$

Here, ϕ represents latitude and Ω represents the rotation rate of the earth, which equals $7.27 \cdot 10^5$ rad/s. By implementing a latitude file, FINEL calculates the Coriolis parameter for the entire model domain.

Boundary conditions

Boundary conditions in the form of water levels can be provided by the TPXO model[1], which provides the 13 principal harmonic constituents of the tide. The TPXO model is a global model of ocean tides, which best-fits, in a least-squares sense, the Laplace Tidal Equations and along track averaged data. The tides are provided as complex amplitudes of sea-surface elevation for eight primary (M_2, S_2, N_2, K_2, K_1, O_1, P_1, Q_1), two long period (M_f, M_m) and 3 non-linear (M_4, M_{S4}, M_{N4}) harmonic constituents, at every quarter degree over the entire ocean. In figure 5.1 it can be seen that the outlines of the model domain follow the shelf break, where this TPXO model is known to be reliable. In figure 5.3 examples are given of time series from this TPXO data that were implemented along the ocean boundary of the ECSM. This figure shows the time series for several points along the ocean boundary, that are indicated in figure 5.4.
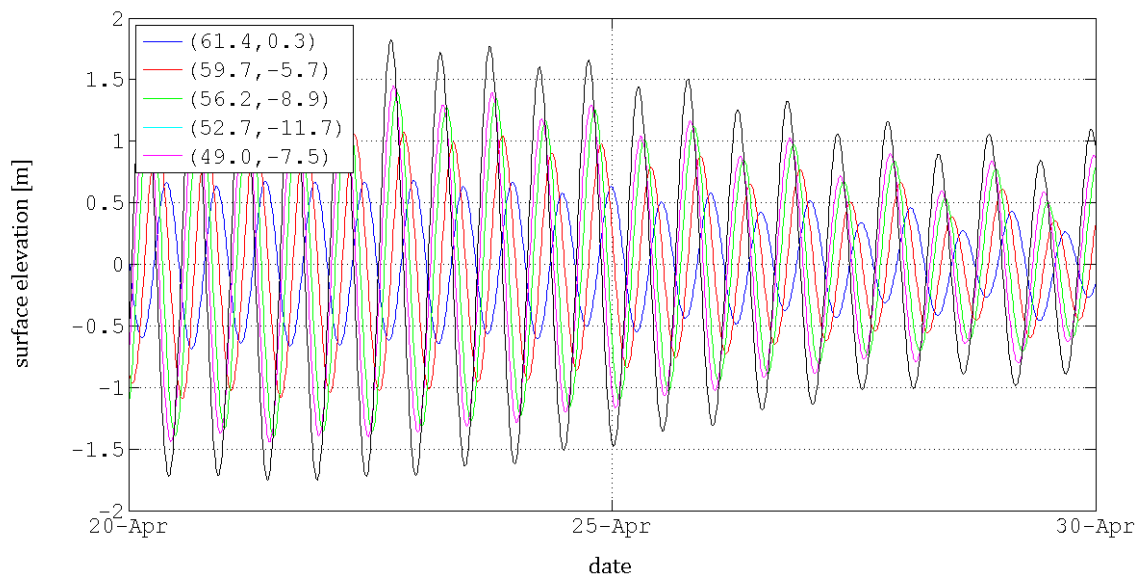

Figure 5.3: *TPXO tidal signals along the ECSM ocean boundary.*

---

[1]http://volkov.oce.orst.edu/tides/global.html

Figure 5.4: *Locations along the ECSM ocean boundary of which TPXO tidal signals are shown in figure 5.3.*

Wind

Since the wind stress is not taken into account in this study, wind data has been studied in order to find a suitable simulation period where wind speeds were low. This data is collected from the European Centre for Medium-Range Weather Forecasts (ECMWF[2]), but also from measurements.

Bottom friction

For the formulation of the bottom friction term the original quadratic settings are used, specifying a Nikuradse roughness $k_N = 0.01$ m, which is a rather low value. The summary of the input used for the ECSM is shown in table 5.1.

Calibration

Despite the fact that the implicit FINEL models are not able to perform parallel calculations , i.e. several processors can be drawn on at the same time, yet, the calculation time for the ECSM model is still limited. The accuracy of the solution depends on the chosen values of Δx and Δt and in fact the stability of the scheme depends on these satisfying the Courant condition:

$$\frac{\Delta t \, c}{\Delta x} < 1 \tag{5.2}$$

Table 5.1: *Input for the ECSM.*

Parameter	Input
Water depth	Bathymetry (see figure 5.2)
Number of layers	Layer every 10 m
Coriolis	Latitude
Turbulence model	Bakhmetev model
Boundary conditions	TPXO harmonic constituents
Wind	None
Bottom friction	$k_N = 0.01$ m

When calculating with an implicit model, the time stepping is less bounded than with explicit. Generally though, the Courant number is a measure for a time step which would not result in an unstable simulation.

5.3 Analytical approach applied onto ECSM

In the preceding chapters the eddy viscosity ν_t, the frequency ω and the water depth d were combined in the dimensionless parameter:

$$\frac{\omega d^2}{\nu_t}$$

Concentrating on the dominant M_2 constituent this parameter can be calculated for all elements within the ECSM model, see figure 5.5. Here, for ν_t a representative constant value of 0.05 m^2/s was chosen. This figure gives insight into typical values of this parameter in practice. For tidal propagation in depths greater than 150 m this parameter exceeds a value of 60, while the central North Sea and English Channel contain values below the 20. Due to reasonable water depths ($\approx$ 100 m) the Irish Sea has pretty high values for $\omega d^2/\nu_t$-parameter.

Also, the dimensionless σ-parameters were defined in the preceding chapters, containing not only the water depth d and the frequency, also a reference velocity $\hat{U}$ and the friction coefficient c_f. Recalling the formula for σ_1 (derived in Chapter 3):

$$\sigma_1 = \frac{8}{3\pi} c_{f1} \frac{\hat{U}}{\omega d}$$

An orienting ECSM simulation was used to estimate this reference velocity $\hat{U}$, resulting in figure 5.6. This figure shows very low values for σ_1, except for the Southern North Sea, the English Channel, several location in the Irish Sea and around the Orkney Islands. Combining these two plots the distribution of the amplitude ratio can be shown for the ECSM, see figure 5.7.
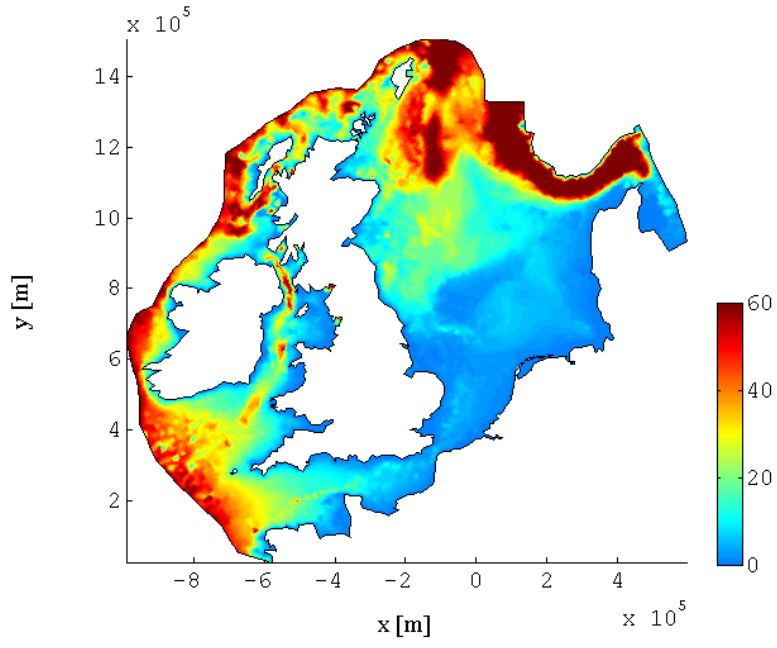
Figure 5.5: $\omega d^2 / \nu_t$ for M_2 with $\nu_t = 0.05\ m^2/s$.

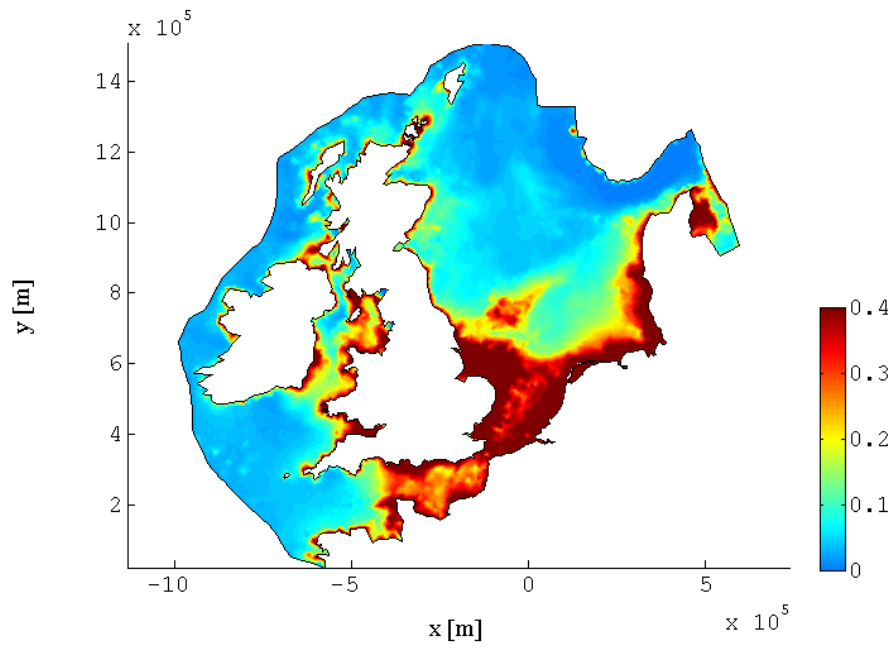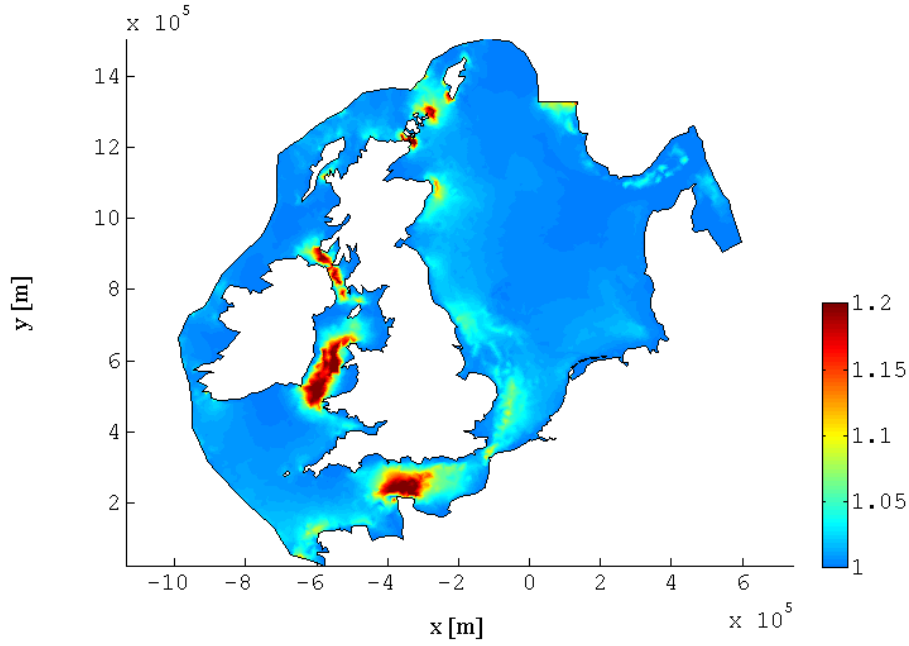Figure 5.6: σ_1 for M_2 with $c_{f1} = 0.002$.

Figure 5.7: *Amplitude ratio for M_2 with $\nu_t = 0.05$ m^2/s and $c_f = 0.002$.*

As figure 5.7 shows, the interesting locations for this study are expected to be the English Channel, the Irish Sea and the Orkney Islands (by applying the analytical approach onto the model). To illustrate in more detail what is happening at those locations, the following figures 5.8 - 5.10 show exactly the same parameters as in figures 5.5 - 5.7, zoomed in on Orkney Islands where the water depth is ≈ 60 m.
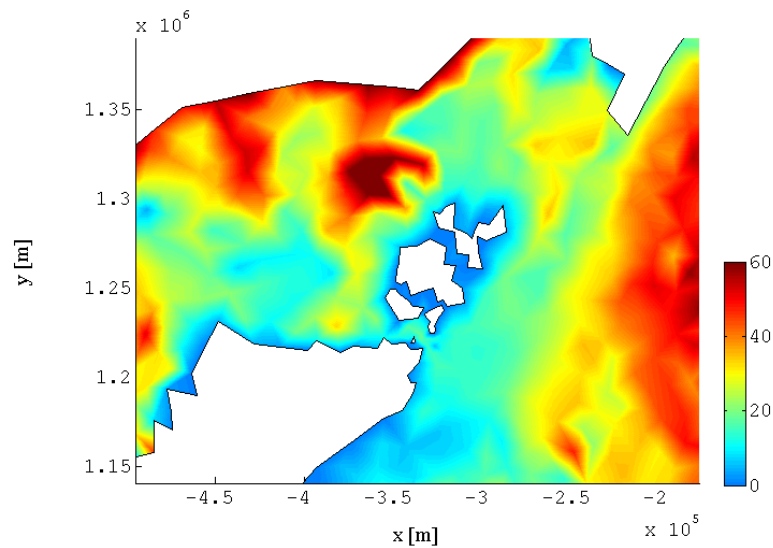

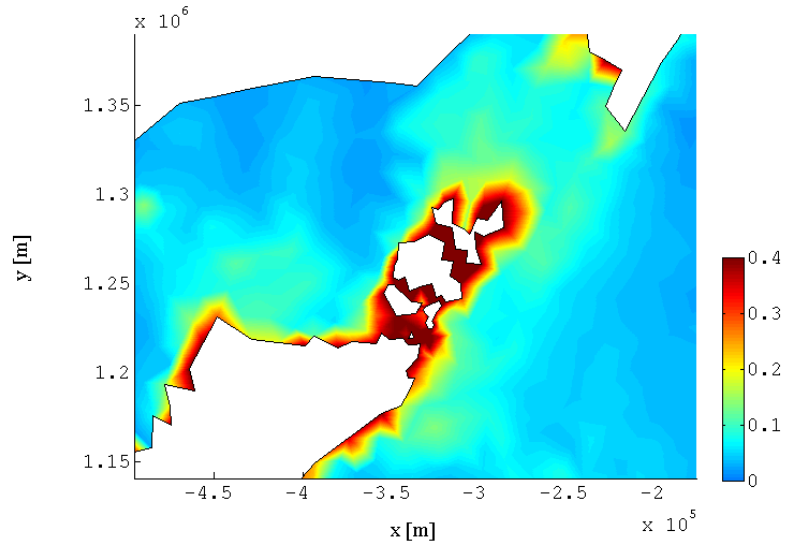Figure 5.8: *$\omega d^2/\nu_t$ for M_2 with $\nu_t = 0.05$ m^2/s, zoomed in on Orkney Islands.*

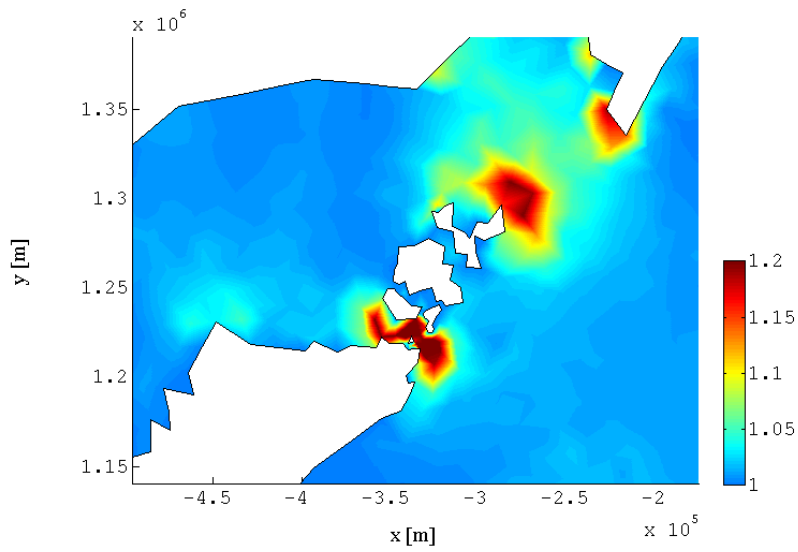Figure 5.9: σ_1 for M_2 with $c_{f1} = 0.002$, zoomed in on Orkney Islands.

Figure 5.10: Amplitude ratio for M_2 with $\nu_t = 0.05$ m^2/s and $c_f = 0.002$, zoomed in on Orkney Islands.

Even though the water is not even that deep at the Orkney Islands, differences of more than 20% are expected here. The $\omega d^2/\nu_t$-parameter is also not very high (≈ 10), but high flow velocities at this location result in a high value for the σ_1-parameter. The high flow velocities are caused by the geometrical contraction.

5.4 Model results

5.4.1 Surface elevation

As a result of the preceding section the model results are studied for specific locations, shown in figure 5.11. These locations include the English Channel, the Irish Sea and the Orkney Islands, as well as 3 locations in the central North Sea.
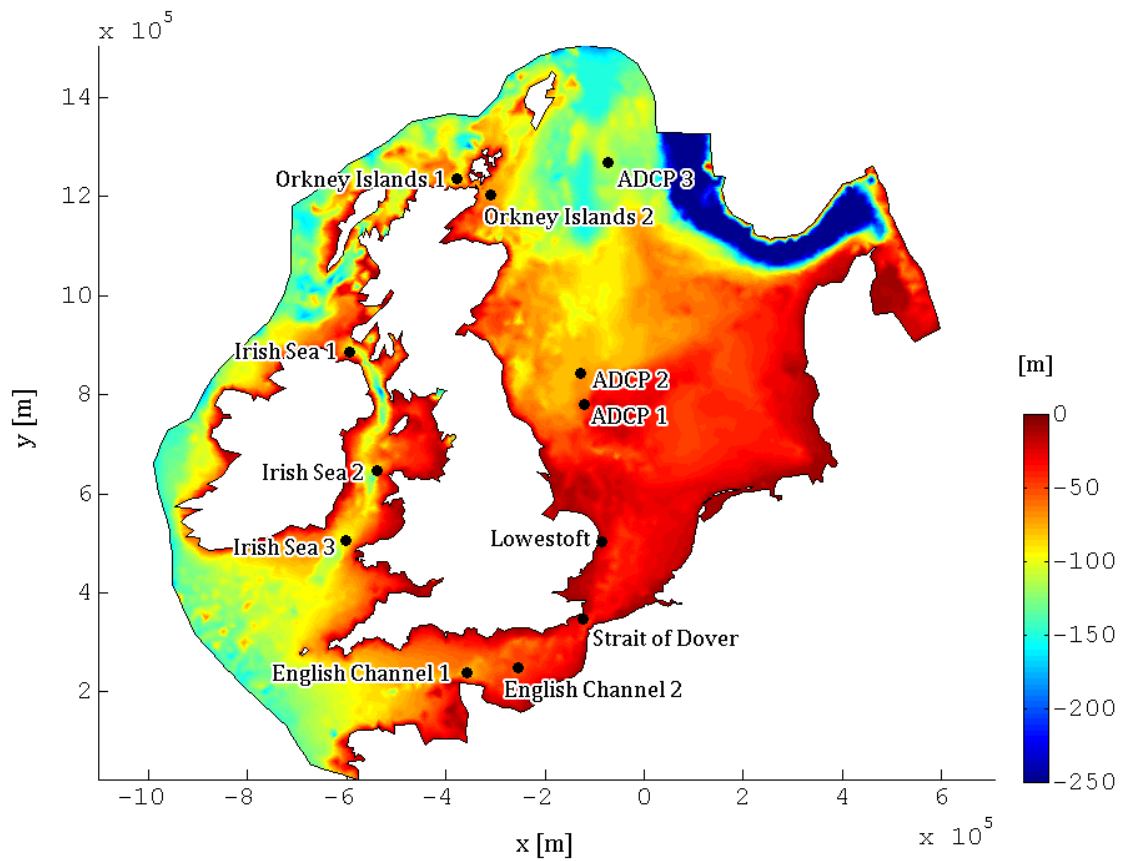

Figure 5.11: *Locations in the ECSM.*

The figures 5.12 and 5.13 show the surface elevation amplitudes, as computed by FINEL2D and FINEL3D respectively. These amplitudes are the maximum surface elevations for every element in 1 day, after a simulation period of 4 days (so after the spin-up time). These plots look very similar in both orders of magnitude as well as the spreading. A more extensive comparison is made by means of timeseries of the FINEL2D and FINEL3D results, see figures 5.14 and 5.15.
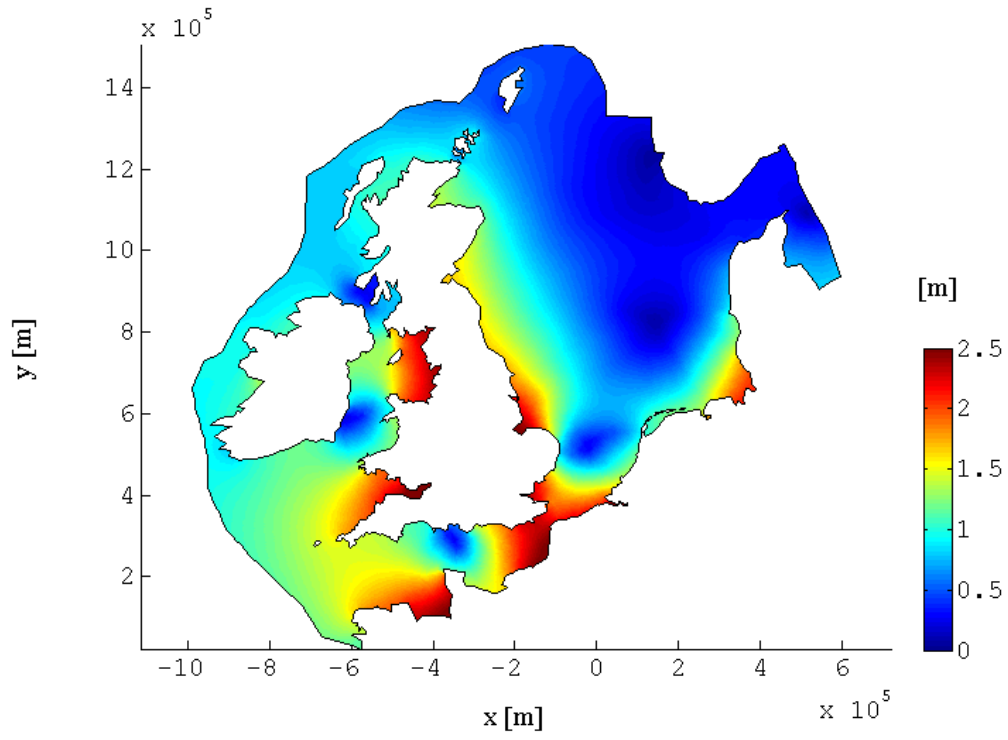
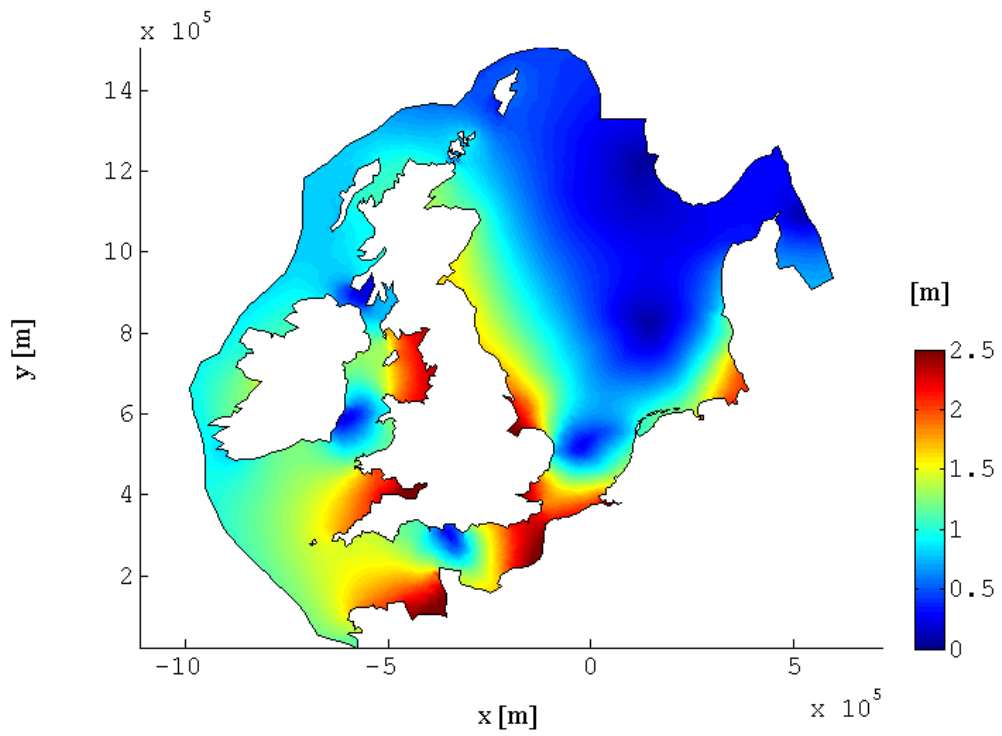Figure 5.12: *Amplitudes of surface elevation calculated by FINEL2D.*

Figure 5.13: *Amplitudes of surface elevation calculated by FINEL3D.*

Globally, the results from FINEL2D and FINEL3D show good correspondence with each other for the surface elevations. Locally, the differences between the results from both models are in the order of a few percentages with observed maxima between $5-10\%$ of the surface elevation amplitude, see table 5.2. In this table the results of the time series of figures 5.14 and 5.15 are summarised by means of the ratio between the amplitudes calculated by FINEL2D and FINEL3D. These amplitudes are determined by taking half the distance between the mean high water and the mean low water, indicated by the dashed lines in the time series plots. There is no actual trend recognised, except for the observation that the 2D signal has larger amplitudes than the 3D signal in most cases.

Table 5.2: *Surface elevation ECSM. The* **ratio** *is the amplitude ratio of the maximum surface elevation in time calculated by FINEL2D and FINEL3D respectively (dashed horizontal lines in figures 5.14 and 5.15.)*

Location	Latitude	Longitude	Depth	**Ratio**
Orkney Islands 1	58°46'N	3°47'W	88 m	1.00
English Channel 1	49°55'N	1°44'W	71 m	0.95
Strait of Dover	51°02'N	1°26'E	55 m	1.01
Lowestoft	52°27'N	1°51'E	31 m	1.04
ADCP 1	54°55'N	1°04'E	53 m	1.01
ADCP 2	55°30'N	0°55'E	81 m	1.02
ADCP 3	59°19'N	1°25'E	110 m	1.03
Irish Sea 2	53°21'N	5°02'W	114 m	1.07

Figure 5.14: *Timeseries of surface elevation as computed by FINEL2D (blue) and FINEL3D (red). The solid horizontal lines indicate the mean surface elevation (2D and 3D); the dashed lines indicate the mean of the surface elevation amplitudes (2D and 3D).*
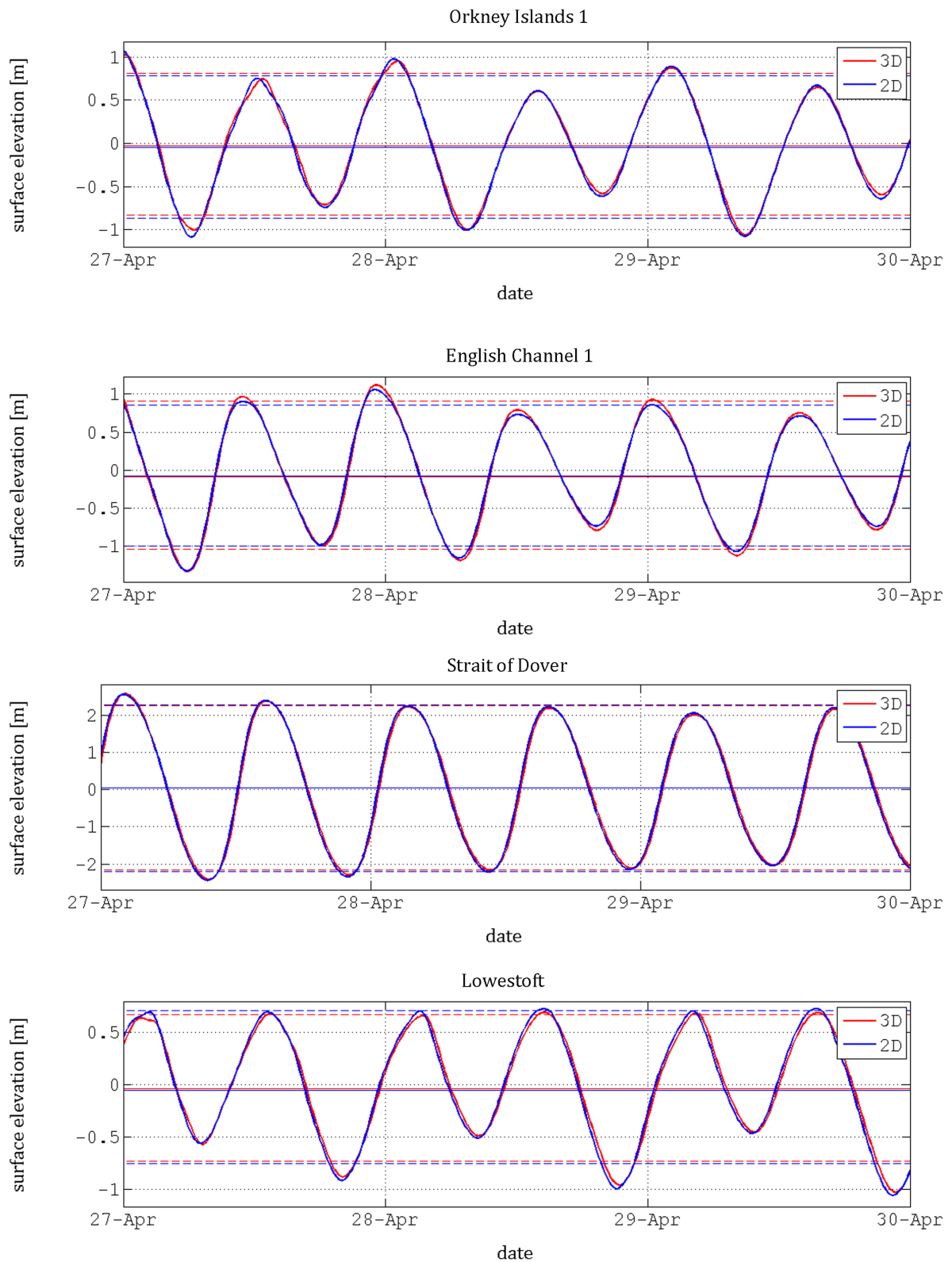
Figure 5.15: *Timeseries of surface elevation as computed by FINEL2D (blue) and FINEL3D (red). The solid horizontal lines indicate the mean surface elevation (2D and 3D); the dashed lines indicate the mean of the surface elevation amplitudes (2D and 3D).*
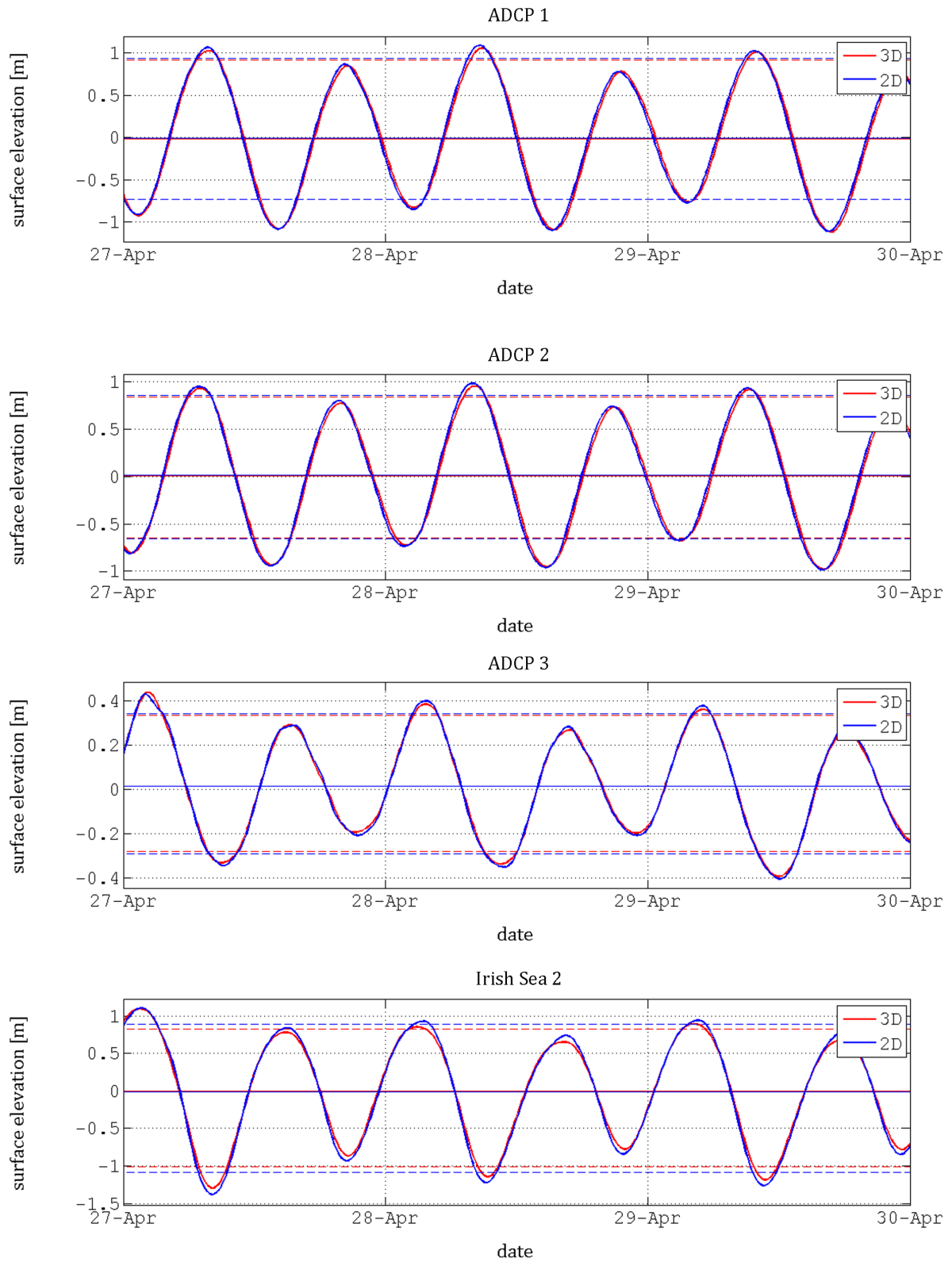
5.4.2 Flow velocities

Figures 5.16 and 5.17 show the maximum amplitudes of the depth-averaged flow velocities, as computed by FINEL2D and FINEL3D respectively. Although the general depth-averaged flow patterns within the 2D and 3D results are very similar, considerable local differences between the 2D and 3D depth-averaged horizontal velocities are found (figure 5.16 is slightly smoother than figure 5.17). Post-processing these results, e.g. to obtain amplitude ratios, this behaviour would be exaggerated. Based on the numerical experiments that have been performed, it can be concluded that the observed behaviour is not caused by numerical instabilities; much rather it is intrinsically linked to the spatial discretization of FINEL, in combination with the very large *aspect ratio* (width/depth ratio) of the 3D tetrahedron elements within this 3D ECSM model. An obvious solution to the problem is to decrease the aspect ratio of 3D elements, which can be achieved by increasing the horizontal resolution. This however would imply an unacceptable increase of computational effort. Another suggestion would be to implement hydrostatic pressure, which is subject for further research.

Since the observed spurious behaviour is not caused by any bug, the general depth-averaged flow patterns within the 2D and 3D results are assumed to be reliable. Ignoring the behaviour, overall differences between 2D and 3D results are the result of the actual physical difference between 2D and 3D models (for, after all, a 2D depth-averaged flow model is a simplification of a 3D flow model in which not all 3D physical effects are present). Locations where differences in 2D and 3D computational results are most likely to occur were indicated by figure 5.7 of section 5.3. According to this figure interesting locations are: the English Channel, the Irish Sea and Orkney Islands, since larger differences between 2D and 3D computational results are to be expected in those regions. For these locations the timeseries are studied, see figures 5.19 and 5.18. The specific locations are indicated in figure 5.11.
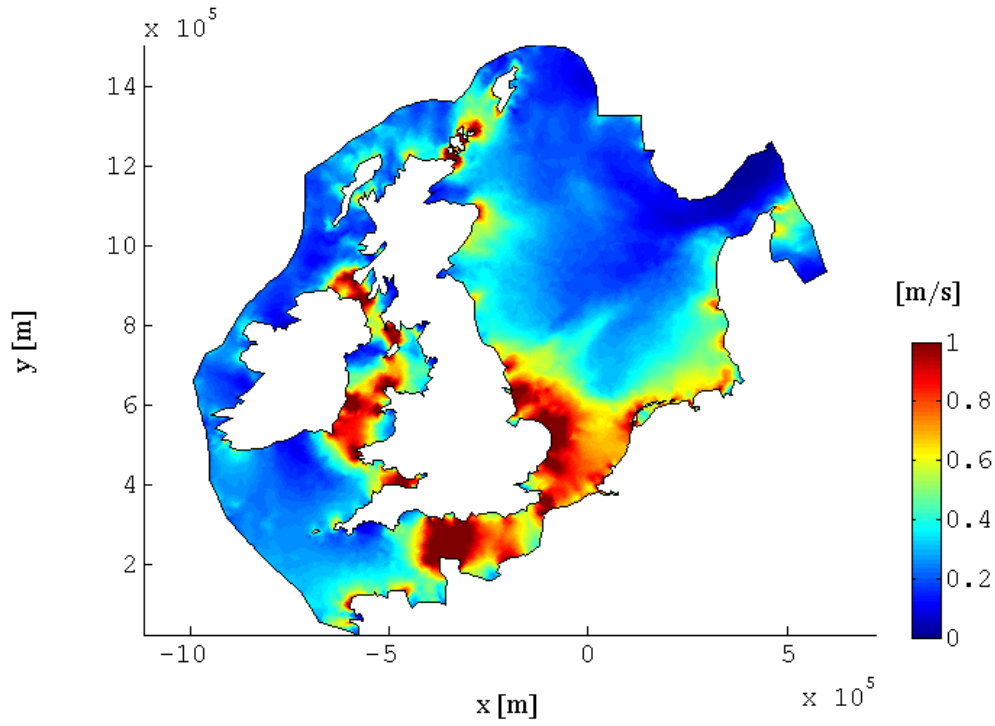
Figure 5.16: *Depth-averaged 2DH flow velocity amplitudes:* $\hat{U}_{2D}$ *calculated by FINEL2D.*
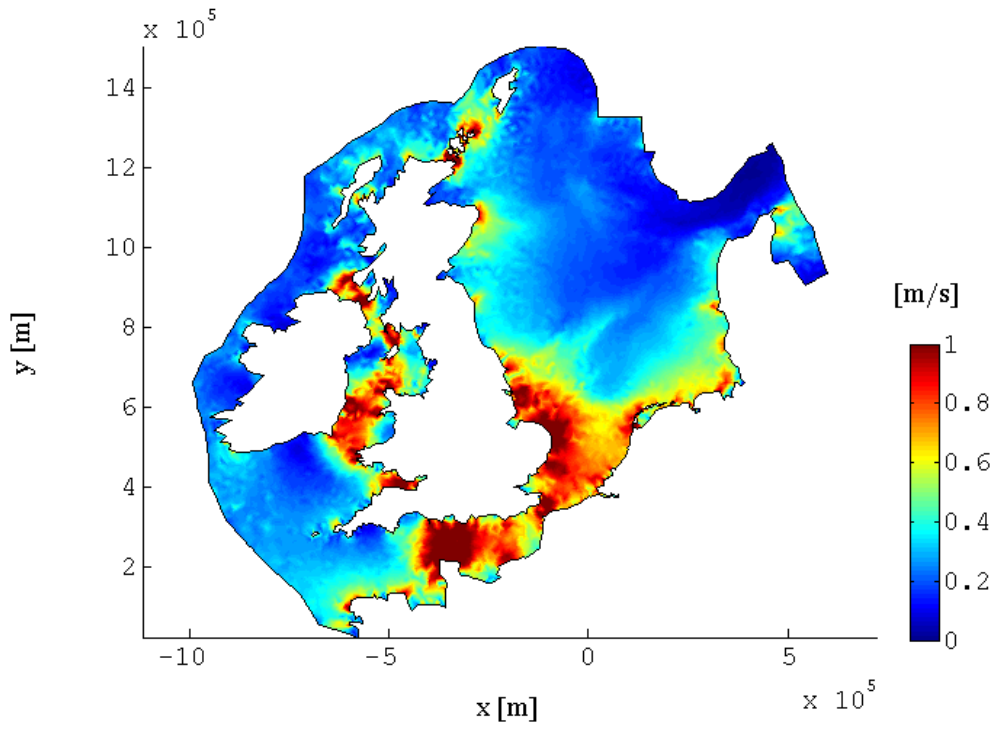

Figure 5.17: *Depth-averaged 3D flow velocity amplitudes:* $\hat{U}_{3D}$ *calculated by FINEL3D.*

The time series of ADCP 1, 2 and 3, representing the central North Sea, show good correspondence between the 2D and 3D results. As was expected from the analytical approach the differences in these regions are within a few percentages. For the locations in the Irish Sea larger differences were expected, which is certainly the case for Irish Sea 1, where the difference reaches over a 50% and 2D and 3D results show very different signals. For Irish Sea 2 the 2D and 3D results correspond surprisingly well (the 3D results are even slightly higher the 2D results). Within the results of Irish Sea 3 interesting behaviour is observed: the 2D signal is alternating much stronger, which results in the 2D alternately peaking over and diving under the 3D signal. Averaged in time it results in a substantial ratio of 1.09 but in reality the difference is even more complex than just this number. The results at the locations in the English Channel also show this behaviour, especially English Channel 1. The time-averaged differences are within a few percentages, but actually the signals deviate strongly. In the Strait of Dover and off the coast of Lowestoft $6-7\%$ deviation is observed. Around the Orkney Islands large differences are found, as was expected, with an extremely high ratio of 1.53 at the location of Orkney Islands 1, so just before the current is constricted by the islands. Apparently, strong differences between 2D and 3D are found in regions where the current is about to meet with complex horizontal geometry and therefore higher flow velocities, which is in line with the expectations and conclusions from the previous chapters.

Table 5.3: *Results ECSM. The **ratio** is the velocity amplitude ratio of the time-averaged maximum flow velocities calculated by FINEL2D and FINEL3D respectively (dashed horizontal lines in figures 5.19.)*

Location	Latitude	Longitude	Depth	Ratio (analytical)	Ratio (numerical)
ADCP 1	54°55'N	1°04'E	53 m	1.01	0.98
ADCP 2	55°30'N	0°55'E	81 m	1.01	1.05
ADCP 3	59°19'N	1°25'E	110 m	1.01	1.05
Irish Sea 1	56°01'N	5°39'W	102 m	1.28	1.52
Irish Sea 2	53°21'N	5°02'W	114 m	1.25	0.99
Irish Sea 3	52°01'N	5°39'W	102 m	1.28	1.09
English Channel 1	49°55'N	1°44'W	71 m	1.29	1.01
English Channel 2	50°05'N	0°20'W	50 m	1.07	0.96
Strait of Dover	51°02'N	1°26'E	55 m	1.10	1.06
Lowestoft	52°27'N	1°51'E	31 m	1.05	1.07
Orkney Islands 1	58°46'N	3°47'W	88 m	1.30	1.53
Orkney Islands 2	58°33'N	2°34'W	73 m	1.39	1.13

Figure 5.18: *Timeseries of depth-averaged flow velocities as computed by FINEL2D (blue) and FINEL3D (red). The solid horizontal lines indicate the mean flow velocities (2D and 3D); the dashed lines indicate the mean of the flow velocity amplitudes (2D and 3D).*
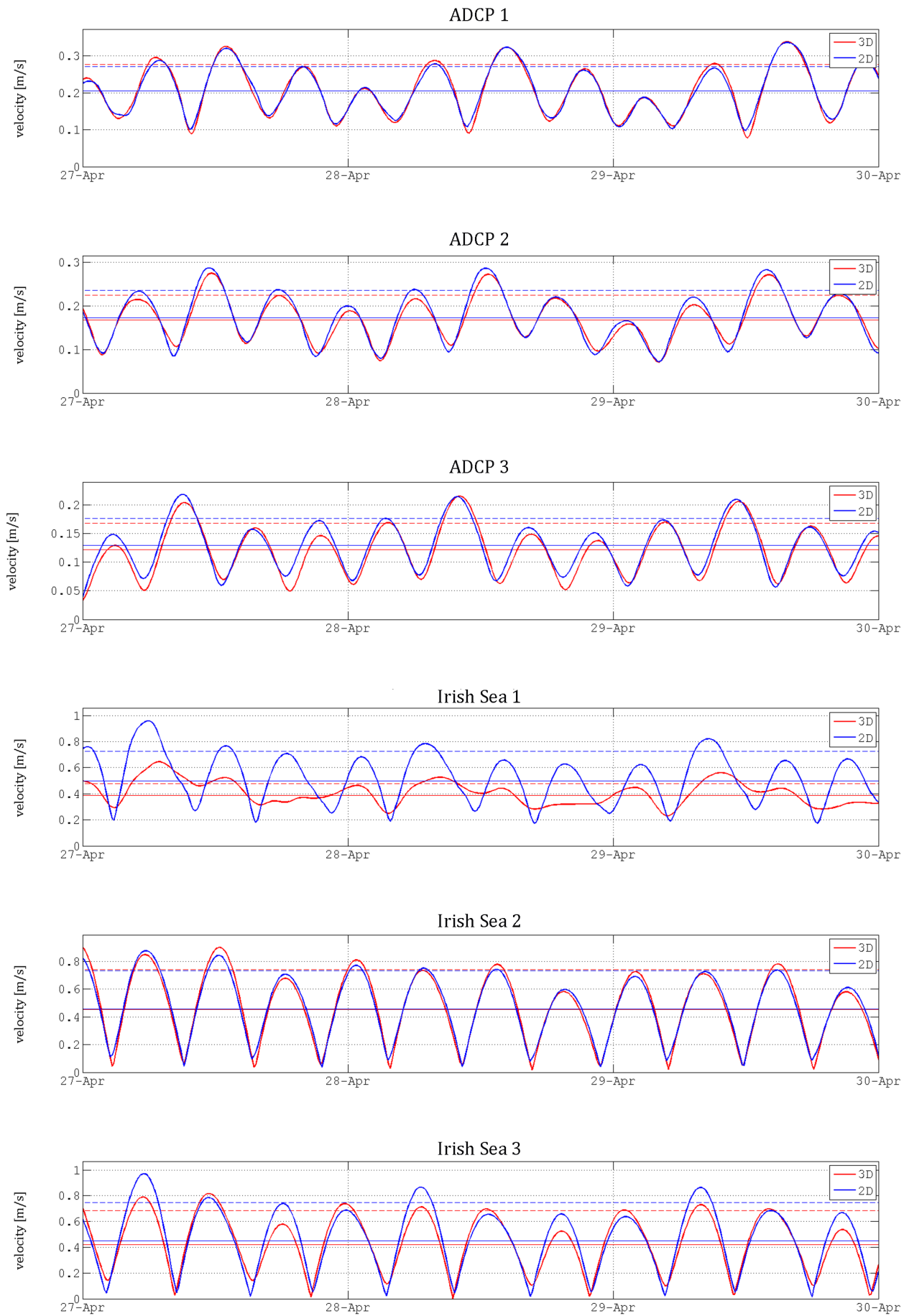
Figure 5.19: *Timeseries of depth-averaged flow velocities as computed by FINEL2D (blue) and FINEL3D (red). The solid horizontal lines indicate the mean flow velocities (2D and 3D); the dashed lines indicate the mean of the flow velocity amplitudes (2D and 3D).*
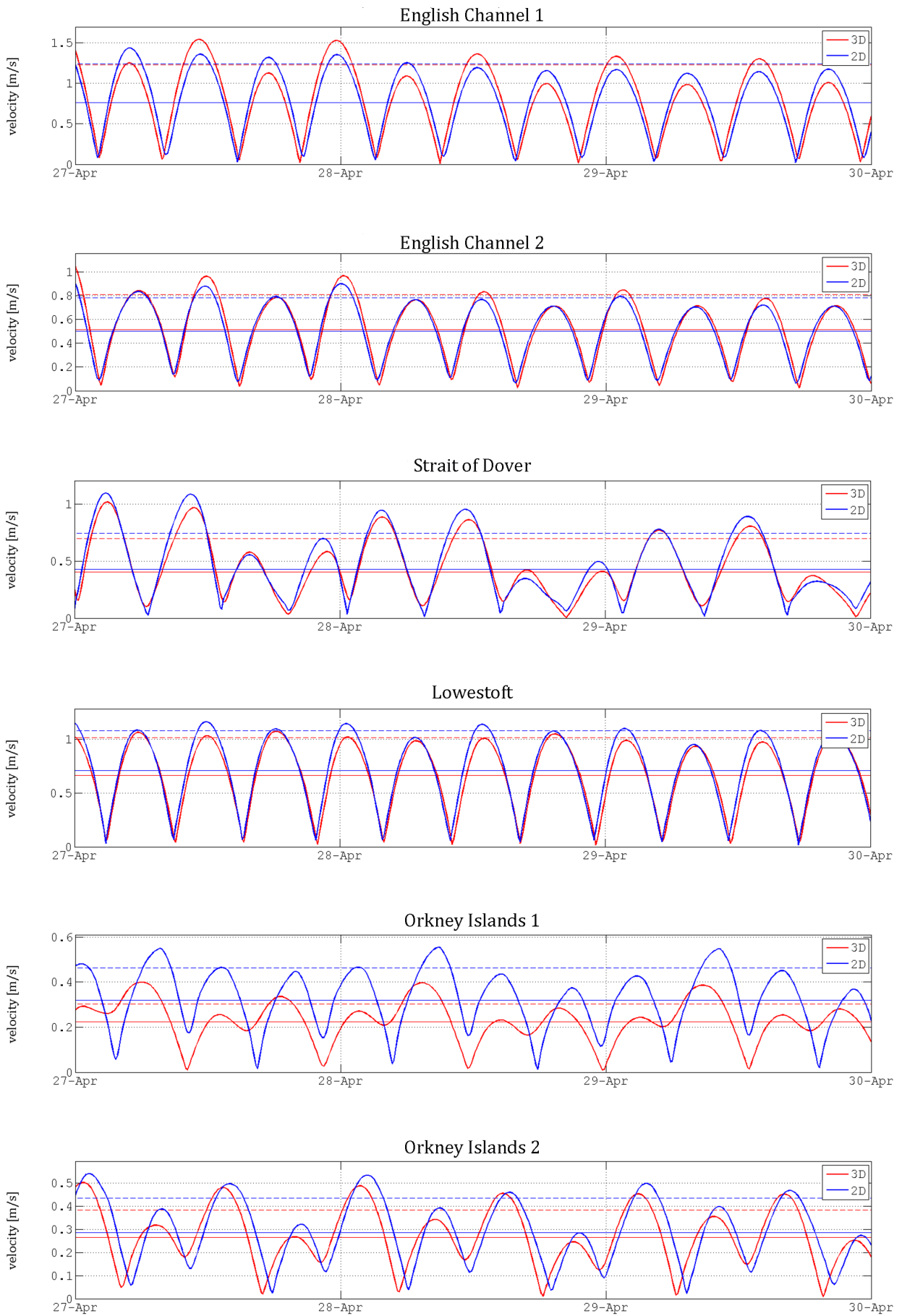
5.5   Discussion

When 3D results are averaged over depth, they can be straightforwardly compared to corresponding results from the 2D model. In general, we observe that 2D and 3D results for the surface elevation are comparable (section 5.4.1), since 2D and 3D results show the approximately identical signals with a maximum difference of $\approx 5 - 10\%$. However, this is not always true for the horizontal velocity components (section 5.4.2), since the 2D simulation may show entirely different signals than the 3D simulation in some cases resulting in differences up to 50%.

Good similarities with theoretical profiles were observed from 2D and 3D results within the schematized rectangular basins of Chapter 4. Due to the very regular character of these geometries and their boundary conditions, the velocity amplitude ratios all lay within a range of a few percentages. For the shelf model of this chapter higher percentages were found. Globally, 2D and 3D ECSM results show great similarities as well. Locally though, differences in especially flow velocities are present. Based on the numerical experiments that have been performed for the ECSM, it can be concluded that the observed differences between 2D and 3D simulations are caused by geometrical constraints in horizontal direction. This actually is in line with the conclusions from the analytical approach, since geometrical constraints may cause relatively high flow velocities. An increase in flow velocity results in an increase of σ, which means that friction becomes more important.

Chapter 6

Conclusions and recommendations

The main objective of this research is to study in which particular instances a depth-averaged model is sufficient to simulate flow processes in a continental shelf sea. In practice, two-dimensional depth-averaged models have proven to be capable of simulating flow and transport processes in for example rivers, lakes or tidal flats. For large-scale continental shelf models though, 3D-behaviour of the flow may become important to take into account. In this chapter conclusions with respect to this behaviour will be discussed and recommendations with respect to further research will be given.

Conclusions

The research questions can be answered with the following conclusions:

- *Which physical processes are relevant in well-mixed continental shelf seas?*

  Shallow well-mixed continental shelf seas like the North Sea are dominated by strong currents produced by tides and storm surges, combined with slowly varying residual currents. This study concentrated on tidal flow neglecting the effects of wind and density differences.

- *Which simplifications are applied to a flow problem in order to allow the use of two-dimensional depth-averaged rather than three-dimensional shallow-water equations?*

  The relevant physical phenomena are described by long waves in a shallow sea with characteristic horizontal length scales much larger than the water depth, which reduces the vertical momentum equation to the hydrostatic balance.

- *Which parameters are important when a depth-averaged model is compared to a model that contains vertical information.*

  Important parameters for processes in shelf seas are: the wave frequency ω, the water depth d, the vertical eddy viscosity ν_t, the flow velocity U and the bottom friction coefficient c_f.

- *In which cases is a depth-averaged two-dimensional model still representative?*

  The answer to this question is found in the following general conclusions.

Based on the literature study, the analytical approach and the numerical experiments that have been performed, the following general conclusions can be drawn:

- This study reveals that the modeller needs to be careful when it comes to two-dimensional depth-averaged hydrodynamic modelling of large-scale domains like the European Continental Shelf Sea.

- The analytical method developed in this study indicates that certain combinations of flow velocities and water depths may cause extensive differences between the results from a depth-averaged model and from a model that contains vertical information. Concentrating on the propagation of the M_2-constituent this method neglects wind, density differences and Coriolis. With a constant vertical eddy viscosity and a certain bottom friction coefficient, the combination of high flow velocities ($\hat{U} > 1$ m/s) and reasonable water depths ($d > 50$ m) may cause substantial deviations. However, those two parameters interact, so conclusions in general sense are hard to quantify.

- The analytical method gives rise to many opportunities and applications. A simple iteration procedure is proposed to investigate what regions in the flow domain may be important. After an orienting 2D calculation a reasonably simple post-processing step should be carried out revealing interesting locations where 2D and 3D results are expected to deviate strongly.

- The numerical simulations show that for tidal propagation in reasonable water depths ($d > 50$ m) and rather low flow velocities ($\hat{U} \approx 0.2$ m/s), bottom and internal friction are of only secondary importance and hence two-dimensional (depth-averaged) models are adequate to calculate flow velocities. This is the case in the central part of the North Sea, which was also predicted by the analytical method.

- Regions where large differences were predicted and observed in the European Continental Shelf Sea model are: the English channel, the Irish Sea and around the Orkneys Islands.

Recommendations

By deriving depth-averaged solutions for the propagation of a tidal constituent, a relationship between the dynamics and bottom shear stress has been established. This relationship is qualified by the omission of the advective, Coriolis and density gradient terms, the linearisation of the friction term, and the absence of wind. However, the presence of significant density gradients or wind stress may radically change the magnitude and vertical distribution of the eddy viscosity and therefore, the current profile. Some recommendations with respect to the analytical approach are given below:

- Coriolis could be implemented in the analytical study by solving the equations of motion with the Coriolis terms taken into account.

- Density differences, caused by pressure, salinity and temperature gradients, can be incorporated in the analytical approach by dividing the system into multiple layers with different densities.

- Wind is very important aspect when considering continental shelf seas like the North Sea. It is therefore recommended to take this into account by either a theoretical study (adding a velocity profile caused by the wind on top of the tidal velocity profile) or with numerical tests.

For the conceptual numerical simulations in a schematized rectangular basin steady and unsteady, periodic flow has been studied. The following case studies are recommended for future research:

- Test the singular progressive wave, analogous to the analytical approach. It would be interesting to study the dampening rate of this wave in the direction of propagation, as computed by a 2D- and a 3D model and compare them to the analytical findings.

- It is recommended to study the amplification factor for a rectangular basin closed in one end and compare them with the analytical findings.

The recommendations concerning the case study of a continental shelf sea model are:

- In order to accommodate the use of FINEL3D for large-scale models like the European Continental Shelf Model it is recommended to implement hydrostatic pressure in the code.

- Apply the analytical method onto other continental shelf sea models to see whether the theory will hold.

Bibliography

Battjes, J., 2002. Lecture notes CT3310 Open Channel Flow. TU Delft.

Deltares, 2013. Delft3D-FLOW User Manual. Deltares, Delft.

Fischer, H., 1979. Mixing in Inland and Coastal Waters. Academic Press, Inc., San Diego.

Holthuijzen, L., 2007. Lecture notes CT5317 Introduction to physical oceanography. TU Delft.

Labeur, R., 2009. Finite element modelling of transport and non-hydrostatic flow in environmental fluid mechanics. Ph.D. thesis, Delft University of Technology.

Labeur, R., Wells, G., 2012. Energy stable and momentum conserving hybrid finite element method for the incompressible navier-stokes equations. SIAM Journal on Scientific Computing, 34(2).

Lorentz, H. A., 1926. Verslag Staatscommissie Zuiderzee. Alg. Landsdrukkerij, Den Haag.

Nieuwstadt, F., 1992. Turbulentie. Epsilon, Utrecht.

Nihoul, J., Ronday, F., 1975. The influence of tidal stress on the residual circulation. Tellus 27.

Pedlosky, J., 1982. Geophysical Fluid Dynamics. Springer-Verlag, Berlin Heidelberg.

Rijkswaterstaat, 2012. Technical documentation WAQUA/TRIWAQ. Rijkswaterstaat.

Uijttewaal, W., 2011. Lecture notes CT5312 Turbulence in Hydraulics. TU Delft.

UnitedNations, 2012. Definition of the continental shelf. United Nations Convention on the Law of the Sea.

Vreugdenhil, C., 1994. Numerical Methods for Shallow-Water Flow. Kluwer Academic Publisher, Dordrecht.

Bottom friction coefficient

In Chapter 3 a comparison is made between the amplitudes and phases of depth-averaged velocities, as computed by a one-dimensional and a two-dimensional model respectively. The outcome of the amplitude and phase ratios appears to be very sensitive to the estimate of the reference velocity $\hat{U}$ as well as to the choice of the bottom friction coefficient c_f. Therefore, the amplitude and phase ratios are plotted again in this Appendix, but now as a function of $\hat{U}$ for two different values of c_f.

Figures 1 and 2 show the velocity amplitude ratio and figures 3 and 4 show the velocity phase ratio, both for a bottom friction coefficient of $c_f = 0.004$ and $c_f = 0.002$ respectively. For certain combinations of tidal constituents (O_1, M_2 and M_4) and water depths (25, 50, 75, 100 m) rather diverse trends are recognised. Concentrating on the propagation of the M_2-constituent in figure 1, it can be seen that the amplitude ratio for the case with a water depth of 50 m is 1.06 (red dot), as was expected since this is exactly the case discussed in Chapter 3. For larger water depths such a deviation would be the case for even lower velocities, and for lower water depths this would be the case for higher velocities. For example, the amplitude ratio reaches almost 45 % for a water depth of 75 m and $\hat{U} = 1.15$ m/s (green dot) while these conditions are not unimaginable for shelf seas. Simirlarly, for a water depth of 100 m the maximum difference of 34 % is reached at a velocity of $\hat{U} = 0.73$ m/s (black dot) which could easily occur in a shelf sea as well. It can be concluded that differences can already be expected at flow velocities of 0.5 m/s, as long as the water depth is reasonably high enough too. Generally, differences are most likely to occur in larger water depths (> 50 m) and higher flow velocities and high velocities (> 0.8 m/s), keeping in mind that those two parameters interact.

Concentrating on the propagation of the M_2-constituent in figure 2, it can be seen that the same amplitude ratios as in the previous case are reached at velocities that are twice as high (red and black dot) because the bottom friction coefficient c_f is twice as low. Velocities that are expected to cause at least a 20% deviation between the velocity amplitudes are given in the table below.

Table 1: *Velocities that are expected to cause at least a 20% deviation in amplitude for two values of the bottom friction coefficient c_f.*

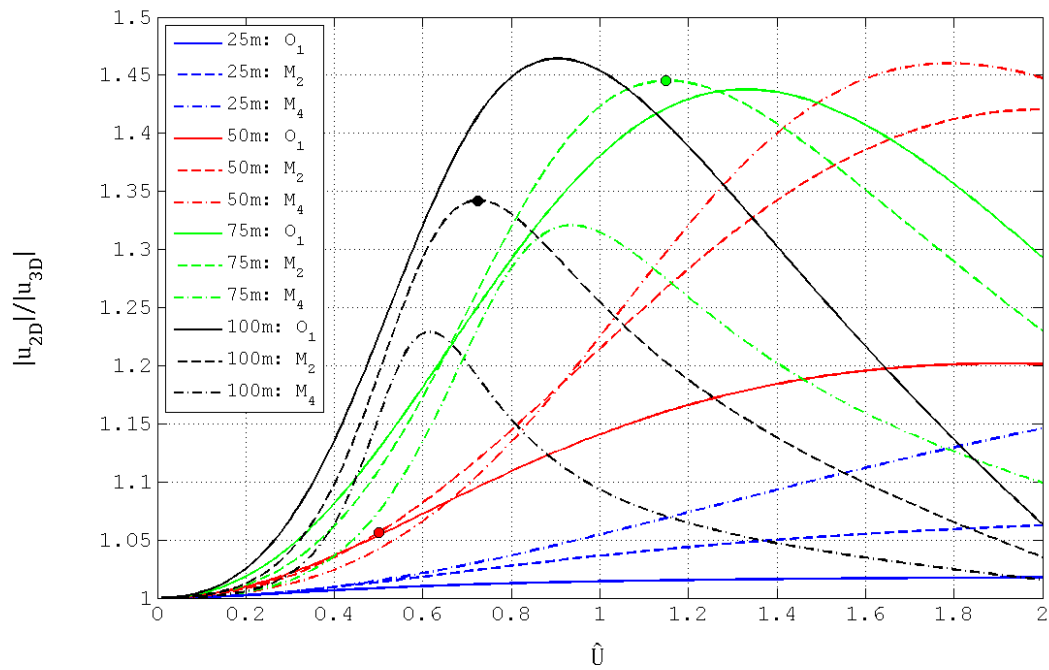| Water depth	$c_f = 0.004$	$c_f = 0.002$
25 m	−	−
50 m	$\hat{U} > 0.9$ m/s	$\hat{U} > 1.9$ m/s
75 m	$0.6 < \hat{U} < 2.1$ m/s	$\hat{U} > 1.2$ m/s
100 m	$0.5 < \hat{U} < 1.2$ m/s	$\hat{U} > 1.0$ m/s

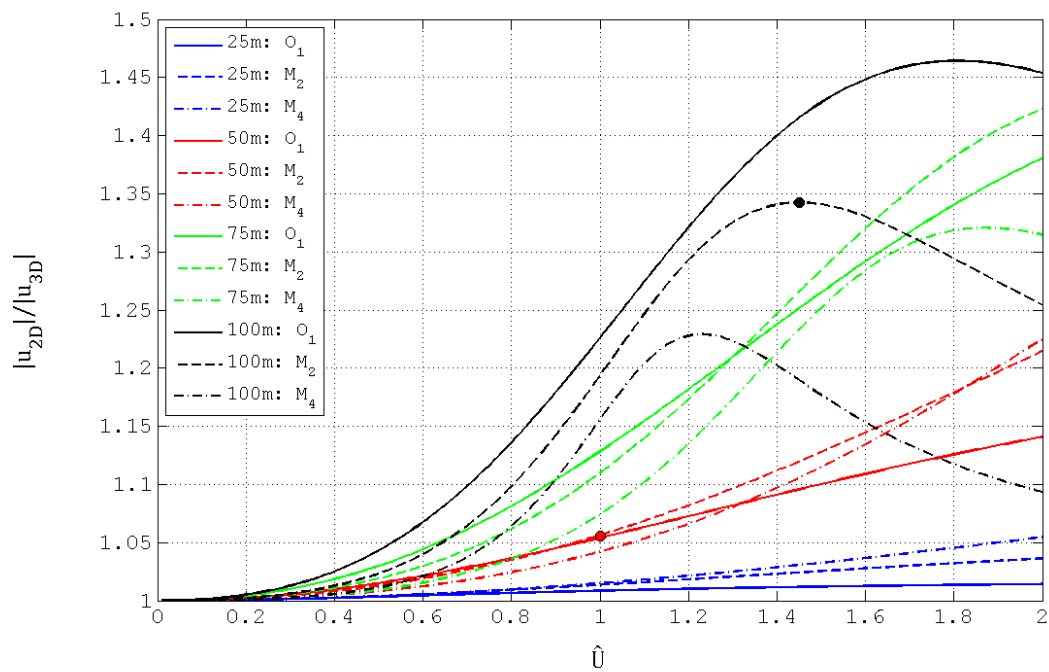Figure 1: *Amplitude ratio between U and $\bar{u}$ as a function of $\hat{U}$ for $c_f = 0.004$.*

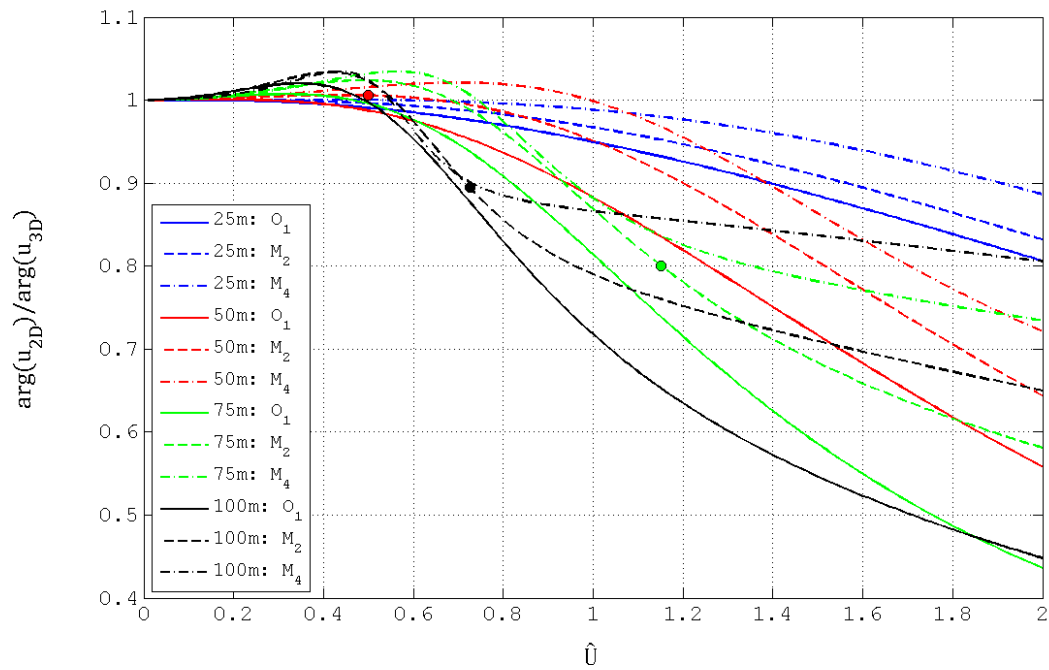Figure 2: *Amplitude ratio between U and $\bar{u}$ as a function of $\hat{U}$ for $c_f = 0.002$.*

Figure 3: *Phase ratio between U and $\bar{u}$ as a function of $\hat{U}$ for $c_f = 0.004$.*
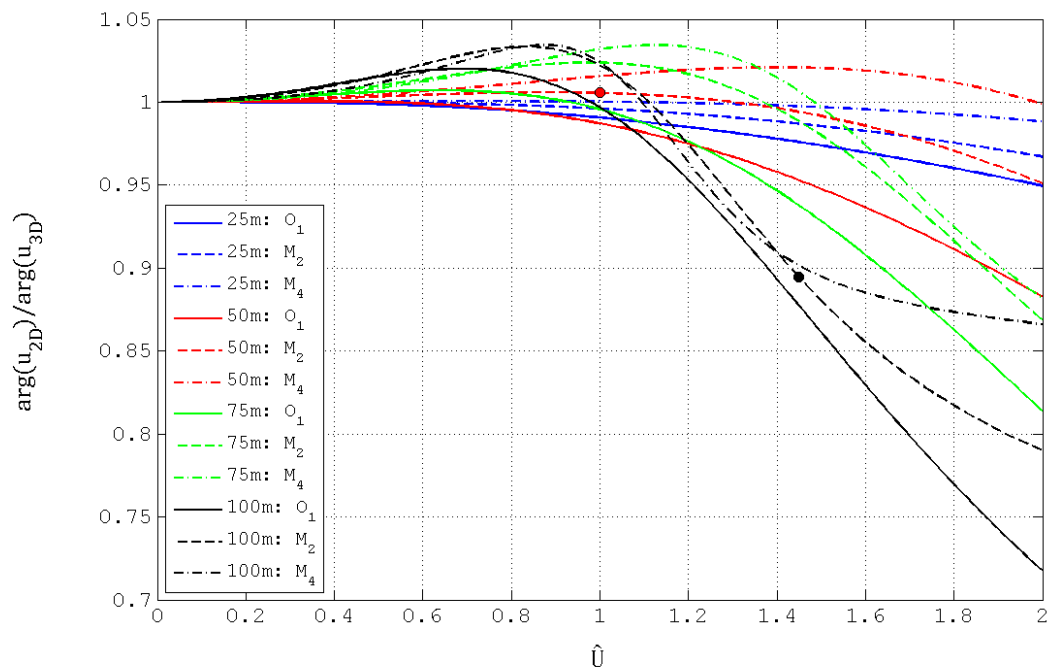

Figure 4: *Phase ratio between U and $\bar{u}$ as a function of $\hat{U}$ for $c_f = 0.002$.*